Inorg. Chem. **2005**, *44*, 7014–7029

Tridentate Copper Ligand Influences on Heme–Peroxo–Copper Formation and Properties: Reduced, Superoxo, and μ-Peroxo Iron/Copper Complexes

Eunsuk Kim,[†] Matthew E. Helton,[†,‡] Shen Lu,[§] Pierre Moënne-Loccoz,[§] Christopher D. Incarvito,[||] Arnold L. Rheingold,[||] Susan Kaderli,[‡] Andreas D. Zuberbühler,[‡] and Kenneth D. Karlin*[,†]

Department of Chemistry, Remsen Hall, Johns Hopkins University, 3400 North Charles Street, Baltimore, Maryland 21218, Department of Chemistry, University of Basel, Basel, Switzerland, Department of Environmental and Biomolecular Systems, OGI School of Science and Engineering at Oregon Health & Science University (OHSU), Beaverton, Oregon 97006, and Department of Chemistry, University of Delaware, Newark, Delaware 19716

Received March 24, 2005

In cytochrome *c* oxidase synthetic modeling studies, we recently reported a new μ-η^2:η^2-peroxo binding mode in the heteronuclear heme/copper complex $[(^2L)Fe^{III}–(O_2^{2-})–Cu^{II}]^+$ (**6**) which is effected by tridentate copper chelation (*J. Am. Chem. Soc.* **2004**, *126*, 12716). To establish fundamental coordination and O_2-reactivity chemistry, we have studied and describe here (i) the structure and dioxygen reactivity of the copper-free compound $(^2L)Fe^{II}$ (**1**), (ii) detailed spectroscopic properties of **6** in comparisons with those of known μ-η^2:η^1 heme–peroxo–copper complexes, (iii) formation of **6** from the reactions of $[(^2L)Fe^{II}Cu^{I}]^+$ (**3**) and dioxygen by stopped-flow kinetics, and (iv) reactivities of **6** with CO and PPh_3. In the absence of copper, **1** serves as a myoglobin model compound possessing a pyridine-bound five-coordinate iron(II)–porphyrinate which undergoes reversible dioxygen binding. Oxygenation of **3** below –60 °C generates the heme–peroxo–copper complex **6** with strong antiferromagnetic coupling between high-spin iron(III) and copper(II) to yield an $S = 2$ spin system. Stopped-flow kinetics in CH_2Cl_2/6% EtCN show that dioxygen reacts with iron(II) first to form a heme–superoxide moiety, $[(EtCN)(^2L)Fe^{III}–(O_2^{-})\cdots Cu^{I}(EtCN)]^+$ (**5**), which further reacts with Cu^I to generate **6**. Compared to those properties of a known μ-η^2:η^1-heme–peroxo–copper complex, **6** has a significantly diminished resonance Raman ν(O–O) stretching frequency at 747 cm^{-1} and distinctive visible absorptions at 485, 541, and 572 nm, all of which seem to be characteristics of a μ-η^2:η^2-heme–peroxo–copper system. Addition of CO or PPh_3 to **6** yields a bis-CO adduct of **3** or a PPh_3 adduct of **5**, the latter with a remaining $Fe^{III}–(O_2^{-})$ moiety.

Introduction

The dioxygen reactivity of small-molecule heme−copper complexes has attracted many synthetic modeling chemists, because such a reaction occurs at the active site of cytochrome *c* oxidases (C*c*Os) for energy production in the respiration of aerobic organisms.[1,2] The binuclear center of C*c*O, where the four-electron/four-proton reduction of dioxygen to water takes place, contains a high-spin histidine-ligated heme (heme a_3) and a tricoordinated copper (Cu_B) in close proximity (∼5 Å). Due to significant contributions from high-resolution X-ray crystal structures[3−11] and exten-

* To whom correspondence should be addressed. E-mail: karlin@jhu.edu. Ph: 410-516-8027. Fax: 410-516-7044.
[†] Johns Hopkins University.
[‡] University of Basel.
[§] Oregon Health & Science University (OHSU).
[||] University of Delaware.

(1) Ferguson-Miller, S.; Babcock, G. T. *Chem. Rev.* **1996**, *96*, 2889−2907.
(2) Michel, H.; Behr, J.; Harrenga, A.; Kannt, A. *Annu. Rev. Biophys. Biomol. Struct.* **1998**, *27*, 329−356.
(3) Iwata, S.; Ostermeier, C.; Ludwig, B.; Michel, H. *Nature* **1995**, *376*, 660−669.
(4) Tsukihara, T.; Aoyama, H.; Yamashita, E.; Tomizaki, T.; Yamaguchi, H.; Shinzawa-Itoh, K.; Nakashima, R.; Yaono, R.; Yoshikawa, S. *Science* **1995**, *269*, 1069−1074.
(5) Tsukihara, T.; Aoyama, H.; Yamashita, E.; Tomizaki, T.; Yamaguchi, H.; Shinzawa-Itoh, K.; Nakashima, R.; Yaono, R.; Yoshikawa, S. *Science* **1996**, *272*, 1136−1144.
(6) Yoshikawa, S.; Shinzawa-Itoh, K.; Nakashima, R.; Yaono, R.; Yamashita, E.; Inoue, N.; Yao, M.; Jei-Fei, M.; Libeu, C. P.; Mizushima, T.; Yamaguchi, H.; Tomizaki, T.; Tsukihara, T. *Science* **1998**, *280*, 1723−1729.

10.1021/ic050446m CCC: $30.25
Published on Web 08/26/2005

Scheme 1

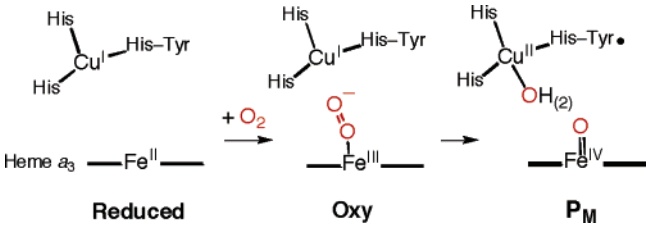

sive kinetic−spectroscopic studies,[12] there is now general agreement on the O_2-binding and reduction products forming during the C*c*O catalytic cycle, Scheme 1. Dioxygen binds to heme a_3, forming the first spectroscopically detectable intermediate, the "oxy" Fe−O_2 adduct. The next observed intermediate contains an O−O bond cleaved moiety, where the fully reduced oxygen atoms derived from O_2 are bound to Cu_B and heme a_3, generating the ferryl−oxo (i.e., Fe^{IV}═O) and Cu^{II}−X (X = OH^- or H_2O) species, "$\mathbf{P}_M$" (Scheme 1).[13,14] However, a full understanding of the O−O bond reductive cleavage process is lacking and many details and insights remain to be determined; these include the role of copper ion and the particulars of its $(His)_2$(His-Tyr) ligation, the possible involvement of a bridging peroxo group (Fe−O−O−Cu) mechanism,[15] peroxo structure (η^2- or η^1- to iron), and proton count and protonation sites during and after O−O cleavage.

As complementary to biochemical and biophysical research, biomimetic chemistry has recently provided well-defined Fe/Cu systems whose coordination chemistry, electrochemical kinetic behavior, and O_2-reaction chemistries are new and serve as important guidelines to understand the C*c*O active site chemistry.[12,16] The exact role of Cu_B and the $(His)_2$-(His-Tyr)−Cu_B center in the heme/Cu/O_2 reaction is especially interesting and important but not resolved. Whereas some biomimetic electrocatalytic studies suggest that copper mainly serves as an electron storage site but does not directly participate in the catalysis,[17] studies from our own and other laboratories have shown that Cu^I or Cu^{II} can directly react with a heme−superoxide (i.e., Fe^{III}−(O_2^-)) or a heme−peroxide to yield bridged heme−peroxo−Cu moieties.[12] The majority of the reported discrete heme−peroxo−copper

Chart 1

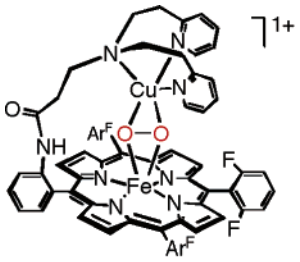

ν(O-O) = 747 cm^{-1}
Fe...Cu = ~3.6 Å

[(^{2}L)Fe^{III}-(O_2^{2-})-Cu^{II}]$^+$ (**6**)

complexes contain a tetradentate copper ligand TMPA moiety, where TMPA = tris(2-pyridylmethyl)amine. One such compound from Naruta and co-workers was crystallographically characterized, demonstrating that the peroxide was bound to iron and copper through an η^2:η^1 fashion.[18] In a recent paper,[19] we reported a dramatically diminished O−O stretching frequency which identified a new type of heme−peroxo−copper complex with a η^2:η^2 peroxo binding geometry (Chart 1). This was achieved by simple change in copper ligand denticity, thus exhibiting the critical nature of the copper ligation in heme−(O_2)−copper complexes, with resulting O−O bond weakening.

In this study, we report details on the formation, physical properties, and small-molecule (CO, PPh_3) reactivities of the heme−peroxo−copper species, [(^{2}L)Fe^{III}−(O_2^{2-})−Cu^{II}]$^+$ (**6**) (Chart 1). The results are discussed in comparison with other known tetradentate heme−peroxo−copper complexes. To compare the observed heme/Cu/O_2 reactions with those of heme/O_2 chemistry, a single iron heme-only complex was also prepared; the X-ray structure of a high-spin five-coordinated ferrous heme and its O_2-binding chemistry are described.

Results and Discussion

Design and Syntheses. To better understand the role of copper ion and influence of copper ligand environment in the heme/Cu/O_2 chemistry, we chose a situation in which the individual heme-only and copper-only chemistries were already quite well understood.

In independent Cu/O_2 chemistry, it is shown that [(L^R)-Cu^I]$^+$ (L = *N*,*N*-bis[(2-(2-pyridyl)ethyl]methylamine, R = H, −OMe, or $-NMe_2$ substituents on the pyridine para positions) react with O_2 to yield [{(L^R)Cu}$_2$(O_2)]$^{2+}$, (η^2:η^2-peroxo)dicopper(II), and bis(μ-oxo)dicopper(III) equilibrium mixtures (as represented by the dotted line O−O moiety in Chart 2).[20−22] These copper−dioxygen adducts perform two-electron oxidations of exogenous substrates, where the more

(7) Ostermeier, C.; Harrenga, A.; Ermler, U.; Michel, H. *Proc. Natl. Acad. Sci. U.S.A.* **1997**, *94*, 10547−10553.
(8) Harrenga, A.; Michel, H. *J. Biol. Chem.* **1999**, *274*, 33296−33299.
(9) Soulimane, T.; Buse, G.; Bourenkov, G. P.; Bartunik, H. D.; Huber, R.; Than, M. E. *EMBO J.* **2000**, *19*, 1766−1776.
(10) Svensson-Ek, M.; Abramson, J.; Larsson, G.; Tornroth, S.; Brzezinski, P.; Iwata, S. *J. Mol. Biol.* **2002**, *321*, 329−339.
(11) Abramson, J.; Riistama, S.; Larsson, G.; Jasaitis, A.; Svensson-Ek, M.; Laakkonen, L.; Puustinen, A.; Iwata, S.; Wikstrom, M. *Nature Struct. Biol.* **2000**, *7*, 910−917.
(12) Kim, E.; Chufán, E. E.; Kamaraj, K.; Karlin, K. D. *Chem. Rev.* **2004**, *104*, 1077−1133.
(13) Hansson, O.; Karlsson, B.; Aasa, R.; Vanngard, T.; Malmstrom, B. G. *EMBO J.* **1982**, *1*, 1295−7.
(14) The source of the fourth electron varies depending on the redox states of the enzyme.[12]
(15) Blomberg, M. R. A.; Siegbahn, P. E. M.; Wikstroem, M. *Inorg. Chem.* **2003**, *42*, 5231−5243.
(16) Collman, J. P.; Boulatov, R.; Sunderland, C. J. *Porphyrin Handb.* **2003**, *11*, 1−49.
(17) Collman, J. P.; Boulatov, R.; Sunderland, C. J.; Fu, L. *Chem. Rev.* **2004**, *104*, 561−588.
(18) Chishiro, T.; Shimazaki, Y.; Tani, F.; Tachi, Y.; Naruta, Y.; Karasawa, S.; Hayami, S.; Maeda, Y. *Angew. Chem., Int. Ed.* **2003**, *42*, 2788−2791.
(19) Kim, E.; Shearer, J.; Lu, S.; Moënne-Loccoz, P.; Helton, M. E.; Kaderli, S.; Zuberbühler, A. D.; Karlin, K. D. *J. Am Chem. Soc.* **2004**, *126*, 12716−12717.
(20) Obias, H. V.; Lin, Y.; Murthy, N. N.; Pidcock, E.; Solomon, E. I.; Ralle, M.; Blackburn, N. J.; Neuhold, Y.-M.; Zuberbühler, A. D.; Karlin, K. D. *J. Am. Chem. Soc.* **1998**, *120*, 12960−12961.
(21) Zhang, C. X.; Liang, H.-C.; Kim, E.-i.; Shearer, J.; Helton, M. E.; Kim, E.; Kaderli, S.; Incarvito, C. D.; Zuberbühler, A. D.; Rheingold, A. L.; Karlin, K. D. *J. Am Chem. Soc.* **2003**, *125*, 634−635.

Chart 2

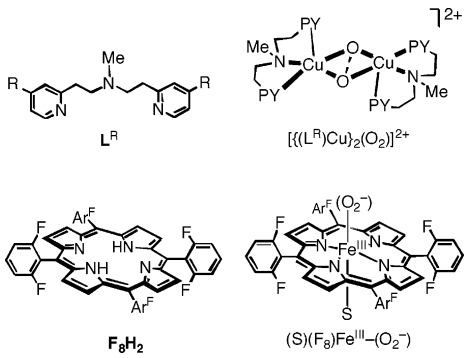

Scheme 2

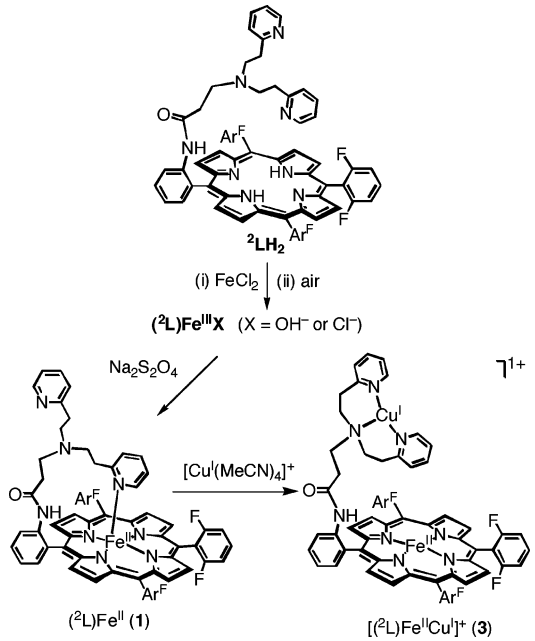

electron-donating R-group provides for faster oxidation rates. On the other hand, in the $(F_8)Fe^{II}/O_2$ reactions, two different O_2 intermediates can be generated depending on the solvent employed. In coordinating solvents such as THF, propionitrile, and acetone, the oxygenation reaction yields oxymyoglobin model compounds, low-spin six-coordinate heme−superoxo complexes $(S)(F_8)Fe^{III}(O_2^-)$ (S = solvent) (Chart 2), whereas a heme−peroxo−heme binuclear $Fe^{III}-(O_2^{2-})-Fe^{III}$ species is generated in noncoordinating solvents such as CH_2Cl_2 or toluene.[23] The heterobinuclear heme−copper complex $[(^2L)Fe^{II}Cu^I]^+$ (**3**) (Scheme 2) contains previously studied $[(L^H)Cu^I]^+$ and $(F_8)Fe^{II}$ moieties, but these two groups are covalently connected in ligand ^2L, leading to new chemistry which cannot be obtained from its individual components.

The general scheme for the preparation of the metal complexes discussed in this report is shown in Scheme 2. Synthetic details for the binucleating ligand $^2LH_2$ and metal complexes were described previously.[19] The deuterated

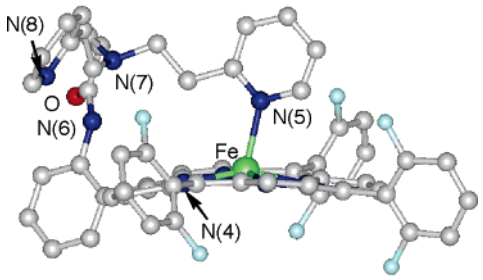

Figure 1. X-ray crystal structure of $(^2L)Fe^{II}$ (**1**). Selected bond distances (Å): Fe−N(5), 2.229; Fe−N(porphyrinate), 2.055−2.080. See also Table 1.

complexes $(^2L\text{-}d_8)Fe^{II}$ (**1**-d_8) and $[(^2L\text{-}d_8)Fe^{II}Cu^I]^+$ (**3**-d_8) were prepared by following the identical procedures for **1** or **3**, except deuterated ligand $^2L\text{-}d_8$ was used for their syntheses, in which $^2L\text{-}d_8$ was synthesized from the deuterated precursor $F_6(NO_2)TPPH_2\text{-}d_8$ (see Experimental Section).

Structure of $(^2L)Fe^{II}$ (1) by X-ray Crystallography and NMR Spectroscopy. X-ray-quality single crystals of $(^2L)Fe^{II}$ (**1**) were obtained from a concentrated acetone solution of **1** at −15 °C. One of the pyridyl arms of the copper chelate was found to be bound to the iron center, giving a high-spin five-coordinated iron complex, Figure 1. These types of synthetic ferrous porphyrinates with an axial base have long been studied to aid in understanding the chemistry of heme proteins such as hemoglobin and myoglobin.[17,24] However, due to the difficulties in preparation of a simple iron porphyrinate containing a single axial base,[25] only a few examples of the X-ray crystal structures of such complexes are known. The structure of **1** (Figure 1 and Figure S1) compares well with other five-coordinate high-spin ferrous heme complexes, as summarized in Table 1. The iron atom is 0.42 Å displaced from the mean 24-atom porphyrin plane (mean deviation is 0.19 Å) toward the pyridyl axial base. The $Fe-N_{py}$ bond length is 2.229 Å, which is longer (0.1−0.2 Å) than other related complexes which contain an imidazole axial ligand (Table 1). Although Fe−N bond lengths may slightly vary due to intrinsic differences between pyridine and imidazole as the N-donor, the elongated Fe−N bond in **1** may be better explained by the repulsion between the porphyrin plane and the tether arm that is connected through the 2-position of the pyridine ring. The steric bulk of the $-CH_2CH_2-$ tether also leads to a tilt of $Fe-N_{py}$ axis that is 13° off from the porphyrin normal axis, most probably to maximize the distance between the methylene hydrogens and the porphyrin core atoms. The distance of the closest hydrogen from the tether arm to a nitrogen of the porphyrin core is 2.66 Å (see Supporting Information Figure S1 for a diagram of **1** from a different perspective).

The ^1H NMR spectrum of **1** exhibited features typical for a high-spin iron(II) porphyrinate with the β-pyrrolic resonances at 51−53 ppm (Figure 2A; also see Figure S5A for a ^2H NMR spectrum). The five-coordinate structure of **1** seems to be retained in solution, as judged by the paramag-

(22) Shearer, J.; Zhang, C. X.; Hatcher, L. Q.; Karlin, K. D. *J. Am Chem. Soc.* **2003**, *125*, 12670−12671.
(23) Ghiladi, R. A.; Kretzer, R. M.; Guzei, I.; Rheingold, A. L.; Neuhold, Y.-M.; Hatwell, K. R.; Zuberbühler, A. D.; Karlin, K. D. *Inorg. Chem.* **2001**, *40*, 5754−5767.
(24) Momenteau, M.; Reed, C. A. *Chem. Rev.* **1994**, *94*, 659−698.
(25) Iron(II) porphyrinate with a single nitrogenous base such as pyridine or imidazole tends to disproportionate to a very stable low-spin six-coordinate species, $(B)_2PFe^{II}$.

Table 1. Selected Bond Distances (Å) and Angles (deg) for Five-Coordinate, High-Spin Iron(II) Porphyrinates

complex	Fe−N_p [a]	Fe−N_{ax}	Δ[b]	θ[c]	ϕ[d]	ref
(^{2}L)Fe (**1**)	2.068	2.229	0.42	13	31.5	this work
[Fe(TPP)(2-MeHIm)]	2.073(9)	2.127(3)	0.38	8.3	24.0	26
[Fe(TpivPP)(2-MeHIm)]	2.072(5)	2.095(6)	0.43	9.6	22.8	27
[Fe(Piv_2C_8P)(1-MeIm)]	2.07(2)	2.13(2)	0.34	5.0	34.1	28
[Fe(TpivPP)(2-MeIm-)]$^-$	2.11(2)	2.002(15)	0.65	5.1	14.7	29

[a] Averaged value. [b] Displacement of iron from the 24-atom mean plane of the porphyrin core. [c] Off-axis tilt (deg) of the Fe−N_{ax} bond from the normal to the porphyrin plane. [d] Dihedral angle between the plane between defined by the closest N_p−Fe−N_{ax} and the pyridine or imidazole plane in deg.

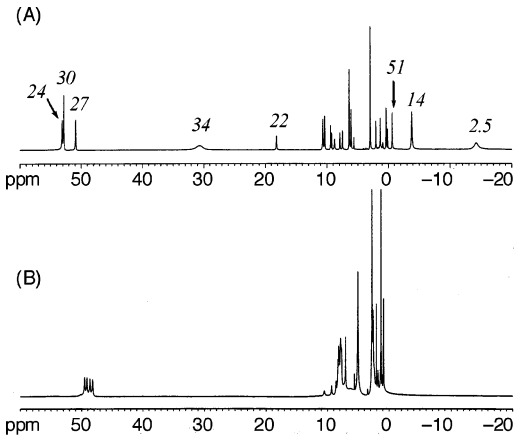

Figure 2. ^{1}H NMR spectra of (A) (^{2}L)Fe^{II} (**1**) and (B) [(^{2}L)$Fe^{II}Cu^{I}$]-$B(C_6F_5)_4$ (**3**) in acetone at room temperature. Some T_1 values (ms) are shown on top of the respective resonances.

netically shifted peaks (31, 18, −0.6, −4, −14 ppm) arising from the metal-bound pyridyl tail; a separate set of resonances in the diamagnetic region (Figure 2A) can be assigned to the noncoordinated pyridyl group.[19] The upfield and downfield shifted resonances were not observed for (F_8)Fe^{II} (Chart 2) which does not contain a pyridyl axial base.[23] The T_1 (≡^{1}H spin lattice relaxation time) values of the paramagnetic resonances in **1** were measured, as noted on top of each peak shown in Figure 2A. Because T_1 is proportional to r^6 (r = the metal−proton distance),[30] T_1 determinations can assist in assigning resonances, where the hydrogens in closer proximity to the metal center have smaller T_1 values. In the NMR spectrum of **1,** the resonance at −14 ppm has a very short T_1 (2.5 ms), whereas the other paramagnetic resonances have T_1 values comparable to those for the pyrrole resonances (Figure 2A). Therefore, we assign the peak at −14 ppm to the hydrogens next to the iron-bound pyridine (i.e., of the −CH_2−pyridyl linker); these are in very close proximity to the iron center (both ∼3.1 Å, determined from the X-ray crystal structure). The chemical shift (−14 ppm) and the T_1 (2.5 ms) value are similar to those for the 6-methyl hydrogens from other high-spin non-heme iron(II)−pyridine complexes such as [Fe^{II}(6-Me_3-TMPA)(CH_3CN)$_2$](ClO_4)$_2$.[31,32] The distances between Fe and the pyrrole hydrogens in the crystal structure are in the range 5.13−5.18 Å, and their T_1 values in NMR spectrum are in the range 24−30 ms. Therefore, one can assume that the peaks at 30, 18, −0.6, and −4 ppm arise from the hydrogens that have comparable metal−H distances to 5.13−5.18 Å. The hydrogens of the bound pyridine (meta and para positions), the ethyl linker (−CH_2-CH_2−pyridyl), and the amide hydrogen from the ligand ^{2}L are good candidates for these resonances, all of which have the Fe−H distances in the range of 5−6 Å. Although further precise assignments for the peaks cannot be made without carrying out further experiments (e.g., specific deuteration), the overall NMR features support a solution five-coordinate structure, consistent with the X-ray crystal structure. We presume dynamic behavior where exchange of one pyridyl axial ligand to the other in ^{2}L could occur, possibly at much higher temperatures.

Dioxygen Reactivity of (^{2}L)Fe^{II} (1). (^{2}L)Fe^{II} (**1**) reacted with dioxygen to form a low-temperature stable superoxo intermediate, thus an oxyhemoglobin or oxymyoglobin model compound, which was monitored by UV−vis and NMR spectroscopy. In CH_2Cl_2 at −80 °C, **1** exhibited UV−vis features at 434 (ϵ = 236 000 M^{-1} cm^{-1}), 534 (ϵ = 8800 M^{-1} cm^{-1}), 555 (ϵ = 9600 M^{-1} cm^{-1}), and 600 (sh) nm (Figure S2). These distinct absorptions in the visible region are characteristic for the iron(II) tetraarylporphyrinates with a single nitrogen axial base.[35] Bubbling of O_2 through solutions of **1** led to new features at 422 (ϵ = 165 000 M^{-1} cm^{-1}) and 542 (ϵ = 16 000 M^{-1} cm^{-1}) nm which were ascribed to a (^{2}L)Fe^{III}−(O_2^-) (**2**), Scheme 3 (and Figures S2 and S3). The UV−vis spectral changes were consistent with the changes of the five-coordinate species transforming to a six-coordinate heme,[35] which was further supported by NMR spectroscopy. ^{2}H NMR spectroscopic studies of the **1**/O_2 reaction were carried out with a deuterated (β-pyrrolic position) complex (^{2}L-d_8)Fe^{II} (**1**-d_8). The reduced complex **1**-d_8 in CH_2Cl_2 had pyrrole resonances at 75 ppm at −80 °C (Figure S4). Oxygenation of this solution resulted in a new

(26) Ellison, M. K.; Schulz, C. E.; Scheidt, W. R. *Inog. Chem.* **2002**, *41*, 2173-2181.
(27) Jameson, G. B.; Molinaro, F. S.; Ibers, J. A.; Collman, J. P.; Brauman, J. I.; Rose, E.; Suslick, K. S. *J. Am. Chem. Soc.* **1980**, *102*, 3224−3237.
(28) Momenteau, M.; Scheidt, W. R.; Eigenbrot, C. W.; Reed, C. A. *J. Am. Chem. Soc.* **1988**, *110*, 1207−1215.
(29) Mandon, D.; Ott-Woelfel, F.; Fischer, J.; Weiss, R.; Bill, E.; Trautwein, A. X. *Inorg. Chem.* **1990**, *29*, 2442−2447.
(30) Bertini, I.; Luchinat, C. *NMR of Paramagnetic Molecules in Biological Systems*; Benjamin/Cummings: Menlo Park, CA, 1986.
(31) Zang, Y.; Kim, J.; Dong, Y.; Wilkinson, E. C.; Appelman, E. H.; Que, L., Jr. *J. Am. Chem. Soc.* **1997**, *119*, 4197−4205.
(32) Although the resonance for the ortho pyridyl hydrogen is expected to appear in downfield region (80−140 ppm) with a very short T_1,[31,33,34] we were not able to detect any such signals under our experimental conditions.
(33) Walker, F. A.; Simonis, U. In *Biological Magnetic Resonance*; Berliner, L. J., Reuben, J., Eds.; Plenum Press: New York, 1993; Vol. 12/NMR of Paramagnetic Molecules.
(34) Walker, F. A. In *The Porphyrin Handbook*; Kadish, K. M., Smith, K. M., Guilard, R., Eds.; Academic Press: San Diego, CA, 2000; Vol. 5/NMR and EPR.
(35) Collman, J. P.; Brauman, J. I.; Doxsee, K. M.; Halbert, T. R.; Bunnenberg, E.; Linder, R. E.; LaMar, G. N.; Gaudio, J. D.; Lang, G.; Spartalian, K. *J. Am. Chem. Soc.* **1980**, *102*, 4182−4192.

Scheme 3

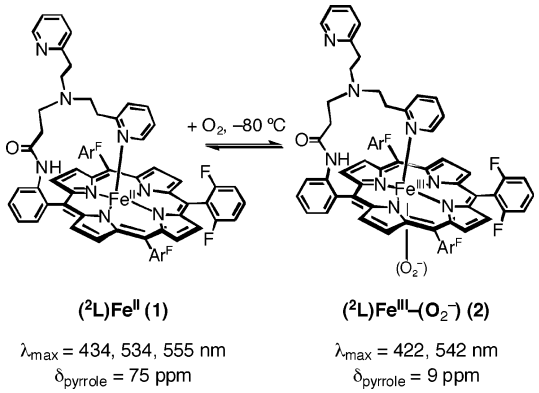

signal at 9 ppm which was attributed to a low-spin six-coordinate heme−superoxo complex, (^{2}L-d_8)Fe^{III}−(O_2^-) (**2**-d_8). Such a heme−superoxo intermediate cannot be generated from the oxygenation of the four-coordinate heme analogue (F_8)Fe^{II} in CH_2Cl_2,[23] indicating that the pyridyl axial ligand in **1** promotes the stable superoxo formation. The O_2-binding to **1** was reversible, where simple Ar bubbling through a solution of **2** with warming yielded **1**. Several cycles of the reversible O_2-binding process could be monitored by UV−vis spectroscopy (Figure S3). Upon warming of the superoxo complex (^{2}L)Fe^{III}−(O_2^-) (**2**) to room temperature in the excess of dioxygen over a long period of time, **2** finally transformed to a hydroxy complex, i.e., (^{2}L)-Fe^{III}−OH with typical spectral features for the heme−hydroxy species with 413 and 571 nm UV−vis features and ∼80 ppm pyrrole resonances in NMR spectroscopy,[36] Figures S2 and S4.

Iron(II)−Copper(I) Complex [(^{2}L)Fe^{II}Cu^{I}]$^+$ (3). Insertion of copper(I) into (^{2}L)Fe^{II} (**1**) (Scheme 2) led to dramatic changes in the ^{1}H NMR spectrum (Figure 2B). Because the copper ion in [(^{2}L)Fe^{II}Cu^{I}]$^+$ (**3**) takes up the tridentate chelate from the ligand ^{2}L, the pyridyl arm is no longer bound to the iron center and the up- and downfield shifted resonances are lost. However, the pyrrole resonances of **3** appeared in a region similar to that seen for **1** in acetone solvent, indicating that complex [(^{2}L)Fe^{II}Cu^{I}]$^+$ (**3**) remained in a high-spin state, now having acetone as an axial ligand base. Since solvent plays a role as an axial base for **3**, the spin state of iron in **3** is solvent-dependent. In weakly coordinating solvents such as acetone or THF the iron maintains a high-spin state, whereas it is low-spin in strongly coordinating solvent like pyridine. In noncoordinating solvents such as CH_2Cl_2 and toluene, iron(II) is four-coordinate and it has an $S = 1$ intermediate spin. The changes in the spin state of **3** in different solvents can be easily monitored by the chemical shifts of the pyrrole resonances;[33,34] the ^{2}H NMR spectra of [(^{2}L-d_8)Fe^{II}Cu^{I}]$^+$ (**3**-d_8) in various solvents are shown in the Supporting Information (Figure S5). Changes in the spin state of **3** in different solvents are also reflected by UV−vis spectroscopy. In CH_2Cl_2, **3** exhibited two bands in the Soret region at 423 and 414 nm, typical for a four-coordinate planar

Scheme 4

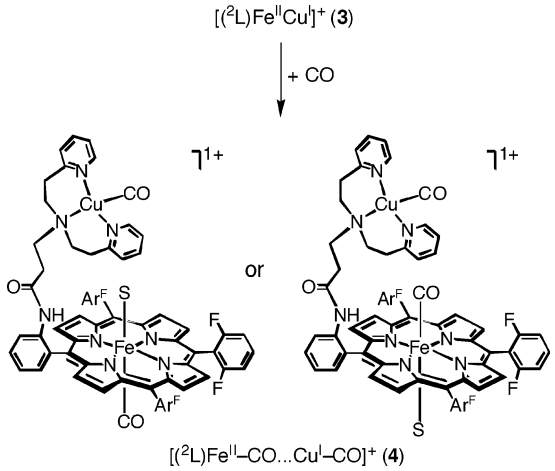

$S = 1$ ferrous heme, whereas it had a single Soret band in THF at 423 nm, indicating that **3** was present as a bis(THF) adduct forming a six-coordinate compound. The X-ray crystal structure of the bis(THF) heme analogue, (F_8)Fe^{II}(THF)$_2$, is known.[37]

Carbon Monoxide Adduct [(^{2}L)Fe^{II}−CO···Cu^{I}−CO]$^+$ (4). In biophysical studies of C*c*O, carbon monoxide has been extensively used to obtain structural and mechanistic insights.[1,6,38−42] In fact, most O_2 intermediates of the C*c*O catalytic cycle are generated from flash photolysis of heme−CO enzyme adducts.[38−41]

The bis(carbonyl) complex [(^{2}L)Fe^{II}−CO···Cu^{I}−CO]$^+$ (**4**) was obtained by bubbling a THF or MeCN solution of [(^{2}L)Fe^{II}Cu^{I}]$^+$ (**3**) with CO (Scheme 4). An immediate color change occurred following reactions of CO with **3** (roughly pink to orange), shown in the UV−vis spectra of Figure 3. A significantly more intense Soret band for **4** appeared (413 nm, $\epsilon = 370\,000$ M^{-1} cm^{-1} in THF) by comparison to that of **3** (423 nm, $\epsilon = 265\,000$ M^{-1} cm^{-1} in THF). ^{2}H NMR spectroscopy revealed that carbonylation of **3** induced changes in the spin state of iron (Figure S5, in Supporting Information). As mentioned earlier, complex **3** is high-spin in THF (Figure S5, B), but the corresponding CO adduct **4** is six-coordinate low-spin, having CO and a solvent THF as axial ligands (Figure S5, E), as seen in many other known heme−CO complexes, including (THF)(F_8)Fe^{II}(CO).[37] Further indication of the solvent binding to the iron in **4** came from solution IR spectroscopy (Figure 3, inset), which revealed the presence of two different C−O stretching bands, one corresponding to the Fe^{II}−CO (1980 cm^{-1}) moiety and the other to the Cu^{I}−CO (2089 cm^{-1}) fragment.[43] The latter value corresponds closely to that known for [(L^H)Cu^{I}−CO]$^+$,

(36) Karlin, K. D.; Nanthakumar, A.; Fox, S.; Murthy, N. N.; Ravi, N.; Huynh, B. H.; Orosz, R. D.; Day, E. P. *J. Am. Chem. Soc.* **1994**, *116*, 4753−4763.

(37) Thompson, D. W.; Kretzer, R. M.; Lebeau, E. L.; Scaltrito, D. V.; Ghiladi, R. A.; Lam, K.-C.; Rheingold, A. L.; Karlin, K. D.; Meyer, G. J. *Inorg. Chem.* **2003**, *42*, 5211−5218.

(38) Proshlyakov, D. A.; Pressler, M. A.; Babcock, G. T. *Proc. Natl. Acad. Sci. U.S.A.* **1998**, *95*, 8020−8025.

(39) Kitagawa, T. *J. Inorg. Biochem.* **2000**, *82*, 9−18.

(40) Han, S.; Takahashi, S.; Rousseau, D. L. *J. Biol. Chem.* **2000**, *275*, 1910−1919.

(41) Szundi, I.; Liao, G.-L.; Einarsdottir, O. *Biochemistry* **2001**, *40*, 2332−2339.

(42) Stavrakis, S.; Koutsoupakis, K.; Pinakoulaki, E.; Urbani, A.; Saraste, M.; Varotsis, C. *J. Am Chem. Soc.* **2002**, *124*, 3814−3815.

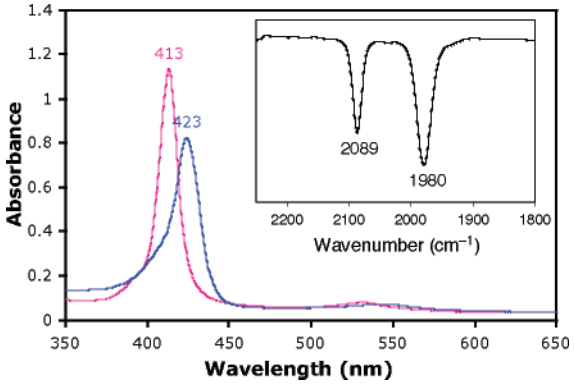

Figure 3. Overlaid UV−vis spectra of $[(^2L)Fe^{II}Cu^I]^+$ (**3**) (blue; 1.5 × 10^{-5} M) and $[(^2L)Fe^{II}-CO\cdots Cu^I-CO]^+$ (**4**) (pink) in THF at room temperature. Inset: difference IR spectrum of **4** minus **3** in acetonitrile.

Scheme 5

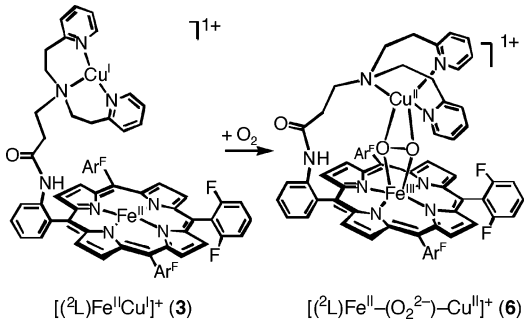

ν = 2089 cm^{-1}.[21] Whereas the copper-bound CO stretching frequencies did not change with variation of solvent, a significant change in the iron-bound CO vibrations occurred. In THF, $\nu(C-O)_{Fe}$ appeared at 1968 cm^{-1}, whereas it occurred at 1980 cm^{-1} in MeCN. The effect must be due to the trans influence of the axial ligand, indicating that iron is six-coordinate with solvent axial base.

Although the Fe−CO and the Cu−CO components are covalently connected to each other, there was no indication of any interaction between them. In fact, the iron(II) and copper(I) carbonyl stretching frequencies are identical with those known for the individual copper-only[21] and the iron-only[37] analogues, $[(L^H)Cu^I(CO)]^+$ and $(THF)(F_8)Fe^{II}(CO)$.

Dioxygen Adduct $[(^2L)Fe^{III}-(O_2^{2-})-Cu^{II}]^+$ (6). As previously reported,[19] reduced iron(II)−copper(I) complex $[(^2L)Fe^{II}Cu^I]^+$ (**3**) binds O_2, resulting in formation of a new type of heme−peroxo−copper complex $[(^2L)Fe^{III}-(O_2^{2-})-Cu^{II}]^+$ (**6**) with a μ-η^2:η^2 peroxo ligation (Scheme 5). Here, we describe spectroscopic data and analyses of **6** which were not fully described in the earlier report, followed by discussions of how these spectroscopic properties compare with those of known tetradentate heme−peroxo−copper complexes, one of which was crystallographically determined to have a μ-η^2:η^1 peroxo binding structure.

(1) Benchtop UV−Vis Spectroscopy. Exposure of THF solutions of **3** to O_2 at −80 °C afforded $[(^2L)Fe^{III}-(O_2^{2-})-Cu^{II}]^+$ (**6**) with UV−vis features at 423 (ϵ = 158 000 M^{-1} cm^{-1}), 484 (ϵ = 11 000 M^{-1} cm^{-1}), and 541 (ϵ = 10 000 M^{-1} cm^{-1}) nm (Figure 4 and Table 2). Application of a vacuum did not affect the stability of the complex, indicating very strong O_2-adduct formation at −80 °C. Similar observations were made in different solvents and solvent mixtures such as acetone, dichloromethane, toluene, CH_2Cl_2/EtCN, and toluene/MeCN; the thermal stability of **6** was observed to be significantly increased in CH_2Cl_2 or toluene as solvent.[44] Upon warming, **6** eventually transforms to a mixture of $Fe^{III}-O-Cu^{II}$ and Fe^{III}−hydroxy species, in analogy to previous observations with many other heme−peroxo−copper complexes.[12] A spectrophotometric O_2-uptake titration (see Experimental Section) for **3** showed that one O_2 molecule binds per dinuclear complex, consistent with the formulation.

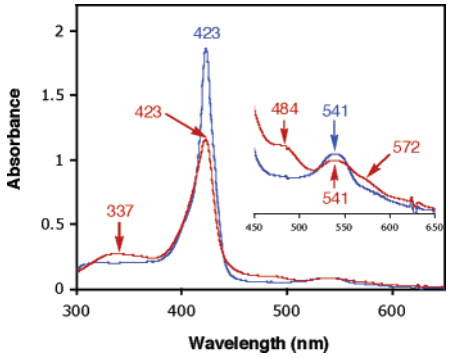

Figure 4. UV−vis spectra of $[(^2L)Fe^{II}Cu^I]^+$ (**3**) (shown in blue; 3.6 × 10^{-5} M) and $[(^2L)Fe^{III}-(O_2^{2-})-Cu^{II}]^+$ (**6**) (shown in red) in THF at −80 °C.

(2) Resonance Raman Spectroscopy. Resonance Raman (RR) spectra of the dioxygen adducts verified that **6** is a peroxo complex in a high-spin heme environment. Soret excitation of $[(^2L)Fe^{III}-(O_2^{2-})-Cu^{II}]^+$ (**6**) at 413 nm resulted in RR spectra dominated by strong porphyrin skeletal modes and weak iron−ligand vibrations. Porphyrin skeletal modes in the high-frequency region of the RR spectra were consistent with a five-coordinate high-spin ferric heme species (ν_4, ν_3, and ν_2 at 1363, 1451, and 1561 cm^{-1}, respectively) as previously observed in the related systems.[45,46] As reported previously,[19] a low-temperature RR spectra of **6** generated in THF with $^{16}O_2$ revealed a ν(O−O) peroxo stretching vibration at 747 cm^{-1} which shifted to 707 cm^{-1} upon $^{18}O_2$ substitution (Table 2). The lack of a splitting at 730 cm^{-1} assigned to the $\nu(^{16}O-^{18}O)$, and observed when **6** is produced with $^{16/18}O$-scrambled O_2 gas suggests a symmetric binding of the peroxo group to the metal center, as in a side-on rather than end-on geometry.[19]

Assignment of the O−O stretching vibrations to a homonuclear dicopper−peroxo species such as $[\{(^2L)Fe^{II}\cdots Cu^{II}\}_2-(O_2^{2-})]^{2+}$ was ruled out because the reaction stoichiometry revealed 1:1 of $O_2/[(^2L)Fe^{II}Cu^I]^+$ (**3**), and the dicopper/O_2 adduct with L^H chelate was known to have a ν(O−O) vibration at 730 cm^{-1} ($\Delta^{18}O_2$ = −39 cm^{-1}, in acetone with 386 nm excitation)[20,47] that was significantly lower than what

(43) Kretzer, R. M.; Ghiladi, R. A.; Lebeau, E. L.; Liang, H.-C.; Karlin, K. D. *Inog. Chem.* **2003**, *42*, 3016−3025.

(44) **6** was stable below −90 °C in THF or acetone, whereas it was stable up to −60 °C in toluene or CH_2Cl_2 solution.

(45) Nakamoto, K. *Infrared and Raman spectra of Inorganic and Coordination compounds*, 5th ed.; Wiley-Interscience: New York, 1997.

(46) Burke, J. M.; Kincaid, J. R.; Peters, S.; Collman, J. P.; Spiro, T. G. *J. Am. Chem. Soc.* **1978**, *100*, 6083−6088.

Table 2. Physical Properties of the Dioxygen Adducts of Heme−Copper Model Complexes

compd	λ_{max}, nm	ν(O−O), cm^{-1} ($\Delta^{18}O_2$, cm^{-1})	ref
	Tridentate Cu−Ligand		
$[(^2L)Fe^{III}-(O_2^{2-})-Cu^{II}]^+$ (**6**)	423, 484, 541, 572 (sh)	747 (−40)	this work
$[(F_8)Fe^{III}-(O_2^{2-})-Cu^{II}(L^{Me2N})]^+$	420, 480, 540, 567 (sh)	767 (−41), 752 (−45)	52
$[(DHIm)(TACNAcr)Fe^{III}-(O_2^{2-})-Cu^{II}]^+$ [a]	428[b]	758 (−18)	53
	Tetradentate Cu−Ligand		
$[(F_8)Fe^{III}-(O_2^{2-})-Cu^{II}(TMPA)]^+$	412, 558	808 (−46)	54
$[(^6L)Fe^{III}-(O_2^{2-})-Cu^{II}]^+$	418, 561, 632	787 (−43)	55
$[tpaCu^{II}-(O_2^{2-})-TPPFe^{III}]^+$	419, 560	803 (−44)	56
$[(TMP)Fe^{III}-(O_2^{2-})-(5MeTPA)Cu^{II}]^+$	420, 557, 612	790 (−44)	18
$[(L^{OH})Fe^{III}-(O_2^{2-})-Cu^{II}]^+$	421, 558, 612	799 (−47)	57
$[(F_8)Fe^{III}-(O_2^{2-})-Cu^{II}(L^{N4}OH)]^+$	417, 560	813 (−44)	58

[a] Iron−porphyrinate moiety also contains an imidazole axial base. [b] Q-band peaks were not reported.

was found in **6**. Additionally, the copper-only O_2 reactions are not likely to cause such big changes in the UV−vis spectra as those which were observed (Figure 4). Similarly, the possibility of the ν(O−O) vibrations coming from a diheme−peroxo species such as $[\{(^2L)Cu^{I}\cdots Fe^{III}\}_2(O_2^{2-})]^{2+}$ was ruled out on the basis of the reaction stoichiometry and NMR spectroscopy (vide infra).[48] While the reaction stoichiometry alone cannot rule out the presence of nonbridged heme peroxo species $[(^2L)Fe^{III}-(O_2^{2-})\cdots Cu^{II}]^+$, such a species would have distinctive EPR signals[49−51] that were not present in **6**. More importantly, such heme−peroxo complexes [(Porphyrinate)$Fe^{III}-(O_2^{2-})]^-$ display a ν(O−O) at significantly higher frequencies (i.e., ∼800 cm^{-1}), [50,51] values much greater than that observed for **6**. Therefore, the RR results in conjunction with reaction stoichiometry as well as UV−vis, NMR, and EPR spectroscopies clearly show that the ν(O−O) at 747 cm^{-1} came from a bridged heme−peroxo−copper species $[(^2L)Fe^{III}-(O_2^{2-})-Cu^{II}]^+$ (**6**).

(3) NMR Spectroscopy. As utilized for the $(^2L)Fe^{II}$ (**1**)/O_2 reaction, low-temperature ^{1}H and ^{2}H NMR spectroscopies were employed to study changes in the structure and the spin state of the iron−copper complexes upon oxygenation. The high-spin reduced compound $[(^2L)Fe^{II}Cu^{I}]^+$ (**3**) in acetone has pyrrole resonances at ∼50 ppm whereas the hydrogen resonances from the d^{10} copper(I) chelate reside in the diamagnetic region at room temperature (Figure 2B). The paramagnetic pyrrole resonances follow Curie behavior as the temperature is decreased, shifting from ∼50 ppm at room temperature (Figure 2B) to ∼95 ppm at −90 °C (Figure 5A). Bubbling dioxygen through a cold solution of **3** led to the formation of $[(^2L)Fe^{III}-(O_2^{2-})-Cu^{II}]^+$ (**6**), whose pyrrole resonances were found at ∼110 ppm. In a separate study, we have reported NMR properties of the mononuclear heme analogues,[23] $(F_8)Fe^{III}-OH$, $(F_8)Fe^{III}-(O_2^{-})$, $[(F_8)Fe^{III}]_2-(O_2^{2-})$, and $(F_8)Fe^{IV}=O$. All of these complexes have

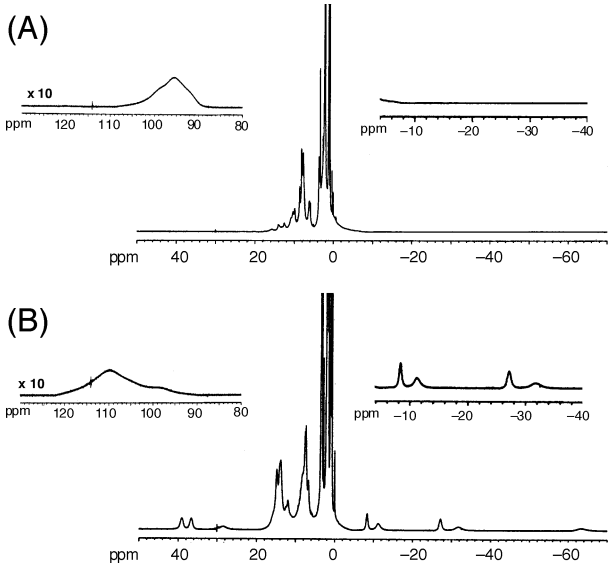

Figure 5. ^{1}H NMR spectra of (A) $[(^2L)Fe^{II}Cu^{I}]B(C_6F_5)_4$ (**3**) and (B) $[(^2L)Fe^{III}-(O_2^{2-})-Cu^{II}]B(C_6F_5)_4$ (**6**) in acetone at −90 °C.

distinctive chemical shifts for the pyrrole hydrogen resonances ($\delta_{pyrrole}$ = 125, 8.9, 17.5, and 3.5 ppm, respectively, at −80 °C); thereby, the pyrrole chemical shifts from **6** allowed us to rule out the possibility of **6** being any of such species.[59] In fact, the 110 ppm pyrrole resonances (−90 °C) are between the ranges known for a pure high-spin Fe^{III} heme

(47) Henson, M. J.; Vance, M. A.; Zhang, C. X.; Liang, H.-C.; Karlin, K. D.; Solomon, E. I. *J. Am Chem. Soc.* **2003**, *125*, 5186−5192.
(48) Peroxo stretching vibrations from homonuclear diheme−peroxo complexes $[(P)Fe^{III}]_2-(O_2^{2-})$ (P = porphyrinate) have not been observed with RR spectroscopy, leaving direct comparison of these data not possible.
(49) Chufán, E. E.; Karlin, K. D. *J. Am Chem. Soc.* **2003**, *125*, 16160−16161.
(50) Burstyn, J. N.; Roe, J. A.; Miksztal, A. R.; Shaevitz, B. A.; Lang, G.; Valentine, J. S. *J. Am. Chem. Soc.* **1988**, *110*, 1382−1388.
(51) Selke, M.; Sisemore, M. F.; Valentine, J. S. *J. Am. Chem. Soc.* **1996**, *118*, 2008−2012.
(52) Kim, E.; Helton, M. E.; Wasser, I. M.; Karlin, K. D.; Lu, S.; Huang, H.-w.; Moënne-Loccoz, P.; Incarvito, C. D.; Rheingold, A. L.; Honecker, M.; Kaderli, S.; Zuberbühler, A. D. *Proc. Natl. Acad. Sci. U.S.A.* **2003**, *100*, 3623−3628.
(53) Collman, J. P.; Herrmann, P. C.; Boitrel, B.; Zhang, X.; Eberspacher, T. A.; Fu, L.; Wang, J.; Rousseau, D. L.; Williams, E. R. *J. Am. Chem. Soc.* **1994**, *116*, 9783−9784.
(54) Ghiladi, R. A.; Hatwell, K. R.; Karlin, K. D.; Huang, H.-w.; Moënne-Loccoz, P.; Krebs, C.; Huynh, B. H.; Marzilli, L. A.; Cotter, R. J.; Kaderli, S.; Zuberbühler, A. D. *J. Am. Chem. Soc.* **2001**, *123*, 6183−6184.
(55) Ghiladi, R. A.; Ju, T. D.; Lee, D.-H.; Moënne-Loccoz, P.; Kaderli, S.; Neuhold, Y.-M.; Zuberbühler, A. D.; Woods, A. S.; Cotter, R. J.; Karlin, K. D. *J. Am. Chem. Soc.* **1999**, *121*, 9885−9886.
(56) Sasaki, T.; Nakamura, N.; Naruta, Y. *Chem. Lett.* **1998**, 351−352.
(57) Liu, J.-G.; Naruta, Y.; Tani, F.; Chishiro, T.; Tachi, Y. *Chem. Commun.* **2004**, 120−121.
(58) Kim, E.; Kamaraj, K.; Galliker, B.; Rubie, N. D.; Moënne-Loccoz, P.; Kaderli, S.; Zuberbühler, A. D.; Karlin, K. D. *Inog. Chem.* **2005**, *44*, 1238−1247.
(59) Although there is 10 °C temperature difference between the current NMR study (−90 °C) and the previous report on the mononuclear complexes (−80 °C), it is extremely unlikely that such a difference can cause a dramatic change in the pyrrole chemical shifts to affect this conclusion.

(∼130 ppm) and the pure high-spin Fe^{II} heme (∼95 ppm) species. This is typical for strongly coupled (porphyrinate)-Fe^{III}−X−Cu^{II} complexes (X = O_2^{2-} or O^{2-}), where strong antiferromagnetic coupling between high-spin Fe^{III} (d^5, S = 5/2) and Cu^{II} (d^9, S = 1/2) leads to a net S = 2 spin system.[54,55,60,61] The S = 2 assignment for **6** was further supported by EPR silent behavior (15 K, in THF/toluene frozen glass) and by a solution magnetic moment determination (μ_{eff} = 5.3 μ_B at −90 °C, in acetone).

Another characteristic feature of the ^{1}H NMR spectrum of **6** is the observable hydrogen resonances from the copper chelate. Generally, it is difficult to observe well-resolved NMR spectra from Cu(II) complexes due to the slow electronic relaxation rate of the Cu^{II} ion.[30] However, in a strongly coupled system like **6**, copper(II) can gain a faster electronic relaxation rate from the electronically coupled Fe^{III}, leading to relatively sharp signals.[61] Complex **6** in Figure 5B exhibits relatively sharp resonances in the upfield (−8, −11, −27, −31 ppm) and downfield regions (39, 37, 29 ppm). By analogy to [(F_8)Fe^{III}−O−Cu^{II}(L^H)]$^+$, whose ^{1}H NMR spectrum was fully assigned,[60] the signals of **6** in the upfield region are believed to originate from the pyridyl hydrogens, whereas the downfield signals at 39, 37, and 29 ppm are due to the methylene H's next to pyridyl donors (−CH_2−PY).[62] Although complete assignment of the NMR spectrum is beyond the scope of interest for this study, the hydrogen resonance assignments for the copper chelate along with the position of the pyrrole resonances support strong antiferromagnetic coupling between Fe^{III} and Cu^{II} through a bridging peroxide ligand.

(4) Comparing and Contrasting the Spectroscopic Properties of Tri- versus Tetradentate Heme−Peroxo−Copper Complexes. There are now several examples of the spectroscopically well characterized heme−peroxo−copper complexes,[18,52−55,63] most of which have a tetradentate ligand TMPA moiety for a copper chelate. These spectroscopic studies of **6** in combination with those from known tetradentate counterparts allow us to get insight into how changes in the peroxo-binding mode enforced by copper ligand denticity can affect their spectroscopic features.

When compared to those of other related heme−peroxo−copper complexes (Table 2), the absorption maxima of complex [(^{2}L)Fe^{III}−(O_2^{2-})−Cu^{II}]$^+$ (**6**) are very similar to those of (F_8)Fe^{III}−(O_2^{2-})−Cu^{II}(L^{Me2N}) (see diagram)[52] but significantly different from those for the group of complexes which have tetradentate copper chelates (Table 2). In the α/β region, complex **6** has two distinctive bands at 484 and 541 nm with comparable extinction coefficients along with a shoulder around 572 nm. However, heme−peroxo−Cu complexes with tetradentate Cu−chelates have a major single band around 560 nm and a minor band with much weaker absorption at ∼610−630 nm.[18,54,55] We presume the differences to alterations in peroxo structures and binding to be imposed by the copper environment (see further discussions below).

Chart 3

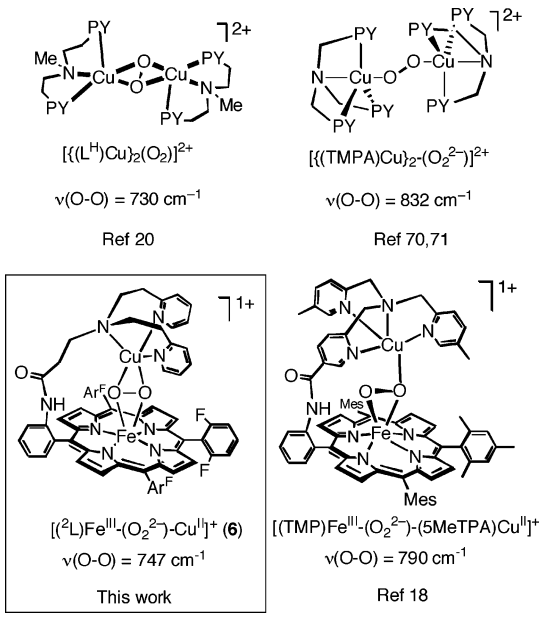

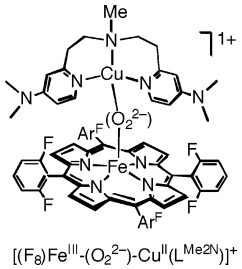

In resonance Raman studies, **6** exhibited a very low ν(O−O) stretching frequency at 747 cm^{-1}, the lowest ν(O−O) frequency among the known heme−peroxo−copper complexes, yet this value is quite close to those of other heme−tridentate Cu complexes (Table 2). On the other hand, all the heme−peroxo−Cu complexes with tetradentate Cu−chelates have significantly higher ν(O−O) values, ca. ∼800 cm^{-1}, that are also very similar to values known for iron(III)-only η^2-peroxo complexes, [(Porphyrinate)-Fe^{III}−(O_2^{2-})]$^-$.[50,51]

In Cu(I)/O_2 chemistry, it is well-known that copper ligand denticity induces different O_2 binding modes.[64,65] Upon dioxygen binding, the Cu(II) centers tend to be five-coordinated, resulting in the tetradentate Cu(I) complexes to favor O_2 binding through an end-on fashion, while ones with tridentate ligands favor the side-on ligation of O_2 (Chart 3). The ν(O−O) stretching frequencies are reflective of the different Cu_2O_2 geometries and resultant bonding in the

(60) Kopf, M.-A.; Neuhold, Y.-M.; Zuberbühler, A. D.; Karlin, K. D. *Inorg. Chem.* **1999**, *38*, 3093−3102.
(61) Nanthakumar, A.; Fox, S.; Murthy, N. N.; Karlin, K. D. *J. Am. Chem. Soc.* **1997**, *119*, 3898−3906.
(62) The methylene H's next to the central amine are expected further upfield, which are not seen here due to the instrumental limit for the spectral window.
(63) Naruta, Y.; Sasaki, T.; Tani, F.; Tachi, Y.; Kawato, N.; Nakamura, N. *J. Inorg. Biochem.* **2001**, *83*, 239−246.
(64) Mirica, L. M.; Ottenwaelder, X.; Stack, T. D. P. *Chem. Rev.* **2004**, *104*, 1013−1045.
(65) Que, L., Jr.; Tolman, W. B. *Angew. Chem., Int. Ed.* **2002**, *41*, 1114−1137.

dicopper(II) peroxo complexes, where the side-on bound peroxides give lower ν(O−O) values (710−760 cm^{-1}) compared to those for end-on peroxides (805−830 cm^{-1}); the former situation is due to a geometry conducive to back-donation from Cu(II) into the σ^* orbital of O_2^{2-}.[66−69] Since peroxide bound to heme−iron(III) is not known to provide these lower ν(O−O) values, it is reasonable to consider that the same inclinations seen in copper−dioxygen binding modes and the resulting ν(O−O) value trends may remain in the heme−peroxo copper systems. Indeed, the X-ray crystal structure of $[(TMP)Fe^{III}-(O_2^{2-})-(5MeTPA)Cu^{II}]^+$ (Chart 3)[18] with η^2:η^1 side-on (to Fe) and end-on (to Cu) peroxo binding contains the TMPA-derivative copper chelate, where the peroxo binding around copper is almost identical with that in $[(TMPA)Cu-O_2-Cu(TMPA)]^{2+}$.[18,70,71]

Despite the large differences in UV−vis and resonance Raman spectroscopic features between tri- and tetradentate heme−peroxo−copper complexs, NMR properties of **6** resemble those of tetradentate counterparts, indicating they all have an $S = 2$ spin system with a strong antiferromagnetic coupling. We do not have in-depth insights for the strong coupling within **6** at this time. However, investigations on the nature of bonding and the origin of strong antiferromagnetic interactions in heme−peroxo−copper complexes just began with one of the tetradentate complexes $[(F_8)Fe^{III}-(O_2^{2-})-Cu^{II}(TMPA)]^+$,[72] and the similar studies with **6** will be conducted in the future.

Kinetics of the $[(^2L)Fe^{II}Cu^{I}]^+$ (3)/O_2 Reaction. The kinetic scheme deduced from stopped-flow spectroscopic analysis for the reaction of $[(^2L)Fe^{II}Cu^{I}]^+$ (**3**) with dioxygen in CH_2Cl_2/6% EtCN is outlined in Scheme 6. This specific solvent system was chosen because EtCN has an influence which is favorable for observation and analysis of the kinetics at temperatures down to −105 °C, and to compare the results of this work with those from a previous investigation on a related system employing 1:1 mixtures of a reduced heme and copper(I) complex with tridentate ligand (L^{Me2N}, Chart 2),[73] see further discussion below.

The UV−vis spectral changes in the α/β region (465−665 nm) of the $[(^2L)Fe^{II}Cu^{I}]^+$ (**3**)/O_2 reaction are shown in Figure 6A over the time period of 0.35 s. At −105 °C, addition of O_2 to **3** resulted in decay of a band at 531 nm (reduced complex **3**) and formation of a transient species

Scheme 6

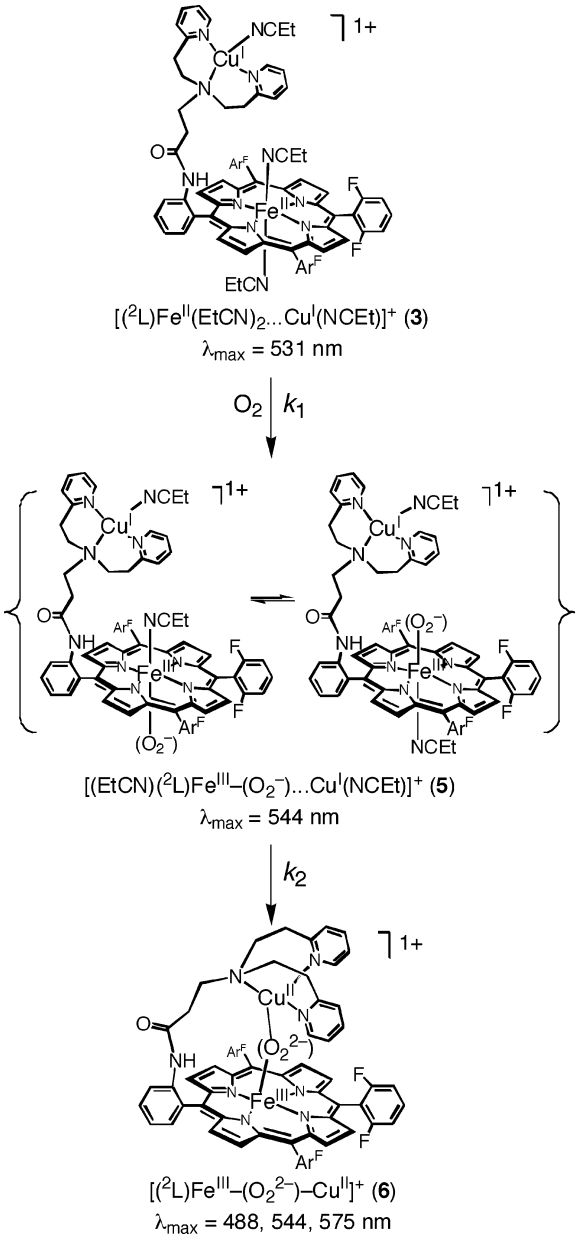

with an absorption at 544 nm, during the first ∼0.03 s. The 544 nm band then decayed over the next 0.3 s and transformed to a spectrum with broad maxima at 488 and 541 nm and a shoulder at 575 nm, i.e., peroxo complex $[(^2L)Fe^{III}-(O_2^{2-})-Cu^{II}]^+$ (**6**). Figure 6A (inset) shows the absorbance versus time traces at 531, 488, and 544 nm, revealing the relationship of formation and disappearance of the various species.

Direct characterization of the transient 544 nm species was not possible due to its extremely short lifetime. However, it formed with a first-order dependence on [O_2] and [**3**], and the UV−vis spectrum of this species (Figure 6B) was very similar to its porphyrin analogues (solvent)$(F_8)Fe^{III}-(O_2^-)$[23,52] and $[(solvent)(^2L)Fe^{III}-(O_2^-)\cdots Cu^{I}(PPh_3)]^+$ (**5**-PPh_3) (Figure 8; see below), allowing us to assign this as a superoxo complex $[(EtCN)(^2L)Fe^{III}-(O_2^-)\cdots Cu^{I}(NCEt)]^+$ (**5**);[74] resonance Raman spectroscopy of the former analogue (solvent)-$(F_8)Fe^{III}-(O_2^-)$, with ν(O−O) = 1178 cm^{-1} and ν(Fe−O)

(66) Ross, P. K.; Solomon, E. I. *J. Am. Chem. Soc.* **1990**, *112*, 5871−5872.
(67) Ross, P. K.; Solomon, E. I. *J. Am. Chem. Soc.* **1991**, *113*, 3246−3259.
(68) Baldwin, M. J.; Ross, P. K.; Pate, J. E.; Tyeklár, Z.; Karlin, K. D.; Solomon, E. I. *J. Am. Chem. Soc.* **1991**, *113*, 8671−8679.
(69) Baldwin, M. J.; Root, D. E.; Pate, J. E.; Fujisawa, K.; Kitajima, N.; Solomon, E. I. *J. Am. Chem. Soc.* **1992**, *114*, 10421−10431.
(70) Jacobson, R. R.; Tyeklár, Z.; Karlin, K. D.; Liu, S.; Zubieta, J. *J. Am. Chem. Soc.* **1988**, *110*, 3690−3692.
(71) Tyeklár, Z.; Jacobson, R. R.; Wei, N.; Murthy, N. N.; Zubieta, J.; Karlin, K. D. *J. Am. Chem. Soc.* **1993**, *115*, 2677−2689.
(72) del Rio, D.; Sarangi, R.; Chufán, E. E.; Karlin, K. D.; Hedman, B.; Hodgson, K. O.; Solomon, E. I. *J. Am. Chem. Soc.* posted ASAP, August 4, 2005; DOI: 10.1021/ja043374r.
(73) Preliminary kinetic studies for the formation of $[(F_8)Fe^{III}-(O_2^{2-})-Cu^{II}(L^{Me2N})]^+$ were previously reported.[52] The fuller analyses for its formation, the k_2 step, are reported here, in the Supporting Information and with results given in Table 3 and Figure 7.

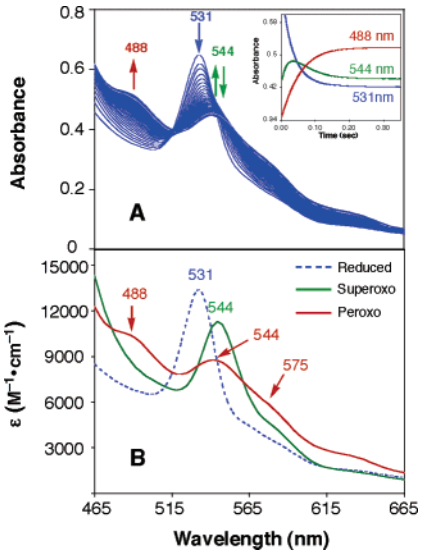

Figure 6. (A) Time-dependent UV−vis spectra of the oxygenation of $[(^2L)Fe^{II}Cu^{I}]^+$ (**3**) at −105 °C in CH_2Cl_2/6% EtCN {concentrations: [**3**] = 2.16×10^{-4} M, $[O_2] = 6.00 \times 10^{-4}$ M}. Inset: absorbance−time traces at 531 nm (blue, decay of **3**), 544 nm {green, formation and subsequent decay of $[(EtCN)(^2L)Fe^{III}-(O_2^-)\cdots Cu^{I}(NCEt)]^+$ (**5**)}, and 488 nm {red, formation of $[(^2L)Fe^{III}-(O_2^{2-})-Cu^{II}]^+$ (**6**)} over ∼3.5 s. (B) Calculated spectra for **3** (blue, λ_{max} = 531 nm), **5** (green, λ_{max} = 544 nm), and **6** (red, λ_{max} = 488, 544, 575 (sh) nm).

= 568 cm^{-1},[52] further supports the formulation as an oxymyoglobin (oxyhemoglobin) model compound. Thus, complex **5** is assumed to be a low-spin six-coordinate iron(III) with one EtCN axial base and a trans superoxide ligand (Scheme 6). Experimentally we cannot distinguish between two possible isomers of the superoxo complex **5** (Scheme 6). If both species were formed in significant amounts, they would have to be in rapid equilibrium. We rule out the possibility that a bis(superoxo) species forms (i.e., $[(EtCN)(^2L)Fe^{III}-(O_2^-)\cdots Cu^{II}-(O_2^-)]^+$) because separate copper-only/O_2 studies showed that the oxygenation chemistry of $[(L^H)Cu^I]^+$ does not occur under these experimental conditions; EtCN strongly suppresses O_2-binding.[75]

The kinetics of the formation of $[(EtCN)(^2L)Fe^{III}-(O_2^-)\cdots Cu^{I}(NCEt)]^+$ (**5**) (Table 3; see Experimental Section for further details) shows that the O_2-binding to iron process is accompanied by a relatively large activation enthalpy (45.3 ± 0.7 kJ/mol) and a large positive activation entropy (120 ± 4 J/(mol·K)). This clearly points to dissociative activation of the process, be it an interchange mechanism with early transition state for loss of EtCN or in fact a fast left-lying equilibrium with reduced coordination number. Similar dissociative processes in the formation of the heme−(O_2^-) species were observed with the analogous untethered systems, $(F_8)Fe^{II}/O_2$ or $(F_8)Fe^{II}/[(L^{Me2N})Cu^{I}]^+/O_2$ (Table 3, Chart 2).[52] Thus, as previously stated,[52] the presence of the copper ion has essentially no influence on the formation of the heme−(O_2^-) species. On the other hand, the rate of formation of this heme−(O_2^-) species in **5** is notably increased (∼10-fold), Table 3. In fact, the activation enthalpy for formation of **5** is a bit larger relative to both the $(F_8)Fe^{II}/O_2$ and $(F_8)Fe^{II}/[(L^{Me2N})Cu^{I}]^+/O_2$ systems, and the enhanced rate comes by way of an increased activation entropy, Table 3. The chemical origin of this effect during the **3**-to-**5** conversion is not entirely clear. By contrast, when other five-coordinate heme complexes such as Collman and co-workers's picket fence porphyrins react with O_2, much smaller activation enthalpies and negative activation entropies are observed;[76] however, they did not employ EtCN, known[23] to be a moderately good ligand for ferrous heme.

The second step, a reaction of the ferric superoxide with a copper(I) species, is of particular interest because such a step or closely related process is key in the O_2-reductive cleavage chemistry in C*c*O (Scheme 1).[1,2] This study in comparison with other related systems (discussed below) shows that the kinetics for the formation of μ-heme−peroxo−Cu species highly depends on the proximity and the ligand architecture of copper (Figure 7). As indicated in Scheme 6 and Figure 6, the transient superoxo species **5** transforms to the μ-peroxo complex $[(^2L)Fe^{III}-(O_2^{2-})-Cu^{II}]^+$ (**6**) on a very fast time scale. Such a heme−peroxo−copper complex formation was not observed with its untethered analogue, $(F_8)Fe^{II}/[(L^H)Cu^{I}(EtCN)]^+/O_2$, wherein only (EtCN)-$(F_8)Fe^{III}-(O_2^-)$ was generated under the same experimental conditions (Figure 7, top). The formation of the untethered "heme−peroxo−copper" species is obtained only after introducing electron-donating groups (NMe_2 donors at para position of the pyridyl groups) to the copper ligand, which makes $[(L^{Me2N})Cu^{I}]^+$ a stronger reductant (Figure 7)[21,52] facilitating binding and reduction of the $(EtCN)(F_8)Fe^{III}-(O_2^-)$ moiety. For the purpose of comparison, the rate constant for the reaction of $(F_8)Fe^{III}-(O_2^-)$ with $[(L^{Me2N})-Cu^{I}]^+$ was made to be pseudo-first-order, arbitrarily using 0.1 mM as the concentration for iron (Table 3 and Figure 7). Under these conditions, despite the electron-donating substituents on the PY2 chelate in L^{Me2N} system, formation of $[(^2L)Fe^{III}-(O_2^{2-})-Cu^{II}]^+$ (**6**) via the *intra*molecular reaction is more than 20 times faster than that for $[(F_8)Fe^{III}-(O_2^{2-})-Cu^{II}(L^{Me2N})]^+$. The formation of **6** and $[(F_8)Fe^{III}-(O_2^{2-})-Cu^{II}(L^{Me2N})]^+$ [73] have essentially identical activation enthalpies (∼36 kJ/mol) for these reactions both involving $Fe^{III}-(O_2^-)$ electron-transfer reduction and binding by copper(I) (Table 3 and Figure 7).[73] We speculate that the differing $\Delta S^{\ddagger}$ values, 54 versus 5 J/(mol·K) (Table 3 and Figure 7) for inter- and intramolecular reactions, respectively, relate to details concerning the process of nitrile dissociation from the Cu^I moiety in each case.

Reactions of $[(^2L)Fe^{III}-(O_2^{2-})-Cu^{II}]^+$(6) with CO and PPh_3. To further probe the nature of the heme−peroxo−copper complex **6**, we carried out initial reactivity studies of **6** with CO and PPh_3. The peroxo complex **6** was generated in situ in THF solution at −95 °C or in toluene/10% CH_3-CN solution at −75 °C. Through the application of vacuum/Ar-purge or freeze−pump−thaw, the excess O_2 was rigorously removed before the reactions with CO or PPh_3. As stated above, dioxygen binding to the reduced complex

(74) The compound number "**5**" is designated to the heme−superoxo/Cu^+ species which possess the ^2L ligand.

(75) Liang, H.-C.; Karlin, K. D.; Dyson, R.; Kaderli, S.; Jung, B.; Zuberbühler, A. D. *Inorg. Chem.* **2000**, *39*, 5884−5894.

(76) Collman, J. P.; Brauman, J. I.; Iverson, B. L.; Sessler, J.; Morris, R. M.; Gibson, Q. H. *J. Am. Chem. Soc.* **1983**, *105*, 3052−3064.

Table 3. Kinetic Parameters for the Formation of Heme−Superoxo (k_1) or Heme−Peroxo−Copper (k_2) Moieties from Fe^{II}/O_2 or $Fe^{II}/Cu^{I}/O_2$ Reactions in CH_2Cl_2/6% EtCN[a]

	$(F_8)Fe^{II}$	$(F_8)Fe^{II}/[Cu^{I}(L^{Me2N})]^+$	$[(^2L)FeCu]^+$ [b]
$Fe^{III}-(O_2^{-})$	k_1, $M^{-1}\,s^{-1}$	k_1, $M^{-1}\,s^{-1}$	k_1, $M^{-1}\,s^{-1}$
168 K	$(4.00 \pm 0.16) \times 10^3$	$(5.7 \pm 0.1) \times 10^3$	$(5.23 \pm 0.04) \times 10^4$
183 K	$(4.86 \pm 0.10) \times 10^4$	$(6.0 \pm 0.1) \times 10^4$	$(8.1 \pm 0.03) \times 10^5$
198 K	$(4.07 \pm 0.16) \times 10^5$	$(4.5 \pm 0.1) \times 10^5$	$(8.4 \pm 0.06) \times 10^6$
ΔH, kJ/mol	41.2 ± 0.6	38.8 ± 0.7	45.3 ± 0.7
ΔS, J/(mol·K)	74 ± 4	63 ± 2	120 ± 4
$Fe^{III}-(O_2^{2-})-Cu^{II}$	NA	k_2,[c] $M^{-1}\,s^{-1}$ (k*, s^{-1})	k_2,[d] s^{-1}
168 K	NA	$(1.28 \pm 0.03) \times 10^4$ (1.28)	$(2.74 \pm 0.04) \times 10^1$
183 K	NA	$(1.16 \pm 0.01) \times 10^5$ (11.6)	$(2.55 \pm 0.03) \times 10^2$
198 K	NA	$(7.6 \pm 0.1) \times 10^5$ (76)	$(1.70 \pm 0.05) \times 10^3$
ΔH, kJ/mol	NA	36.2 ± 0.2	36.6 ± 0.4
ΔS, J/(mol·K)	NA	54 ± 1	5 ± 0.4
ref	52	52 and this work	this work

[a] Notes: uncertainties given are as standard errors. [b] From analysis of data taken from 168 to 179 K. [c] From analysis of data taken from 168 to293 K. [d] From analysis of data taken from 168 to 191 K. NA = not applicable. k* calculated as pseudo-first-order assuming 0.1 mM concentration for iron.

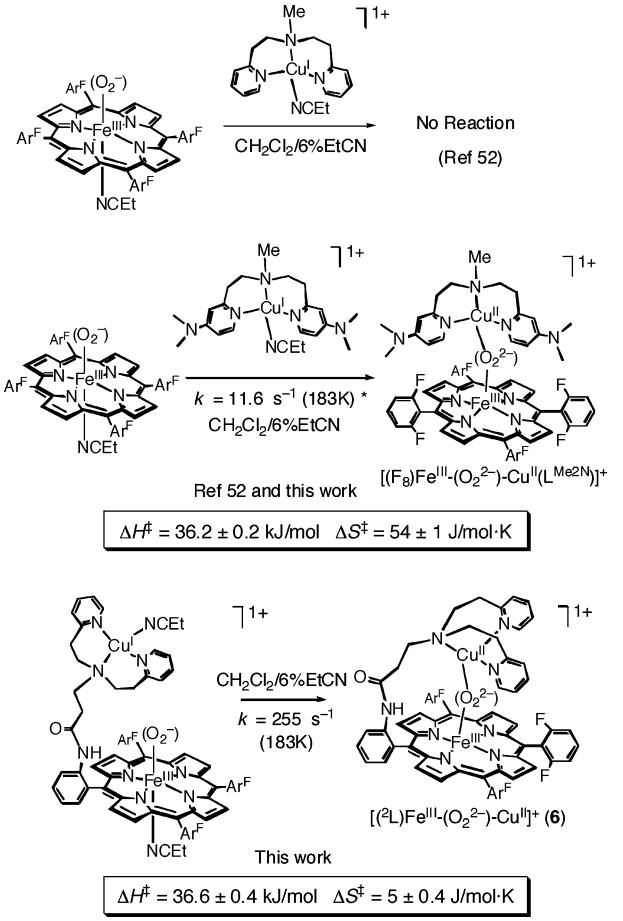

Figure 7. Comparisons of kinetic parameters for formation of heme−peroxo−copper species.[52] Asterisk indicates calculated as pseudo-first-order assuming 0.1 mM concentrations for iron. See text.

Scheme 7

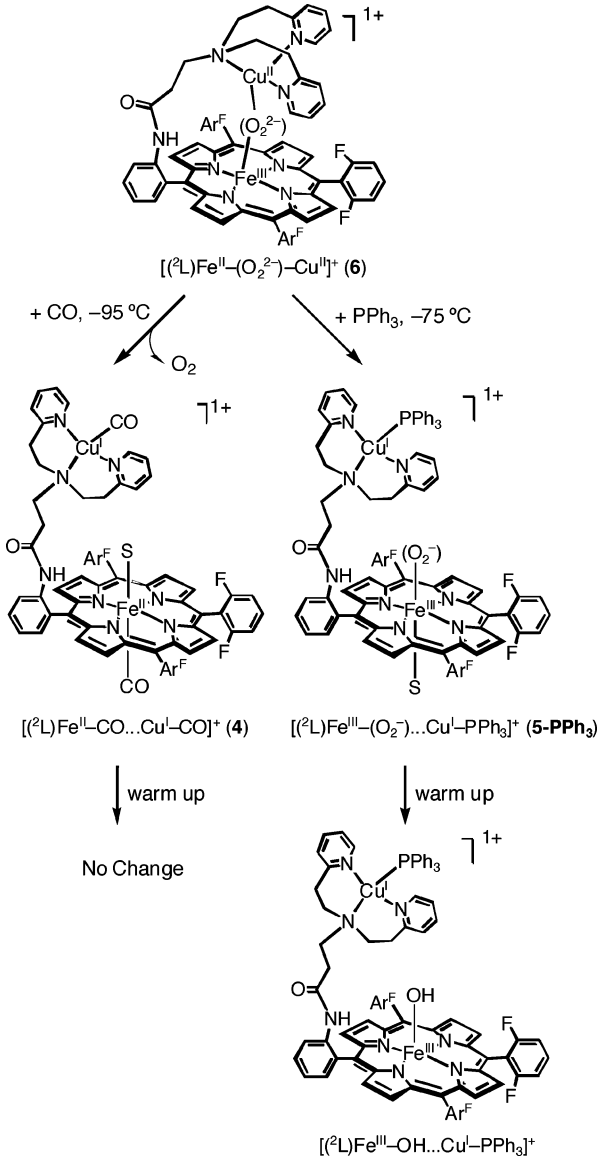

$[(^2L)Fe^{II}Cu^{I}]^+$ (**3**) was not reversed by simple vacuum/Ar-purging. However, the peroxo complex **6** was found to react with CO to form the reduced $Cu^{I}-CO$ and $Fe^{II}-CO$ complex with concomitant liberation of dioxygen (Scheme 7). When CO was bubbled through a THF solution of **6** (−95 °C), immediate UV−vis spectral changes occurred with formation of features at 413 and 532 nm which were identical with those generated by independent formation of $[(^2L)Fe-CO\cdots Cu-CO]^+$ (**4**) through CO exposure to $[(^2L)Fe^{II}Cu^{I}]^+$ (**3**); vide supra. Solution IR spectra confirmed the presence of the bis(CO) compound, revealing two ν(C−O) vibrations at 2089 and 1968 cm^{-1} (see Supporting Information, Figure S7). The amount of O_2 evolved (~70%) was semiquantified using a detection procedure employing an alkaline pyrogallol

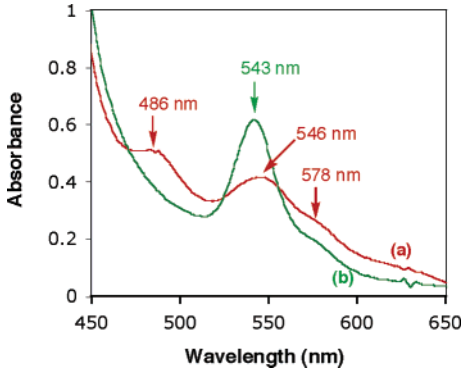

Figure 8. UV−Vis spectra of the reaction of $[(^2L)Fe^{III}-(O_2^{2-})-Cu^{II}]^+$ (**6**) with PPh_3 in toluene/10% CH_3CN at −75 °C: (a) spectrum of **6** generated by bubbling $[(^2L)Fe^{II}Cu^{I}]^+$ (**3**) with O_2 (shown in red, λ_{max} = 486, 546 nm); (b) spectrum of $[(CH_3CN)(^2L)Fe^{III}-(O_2^{-})\cdots Cu^{I}(PPh_3)]^+$ (**5**-PPh_3) generated by the reaction of **6** with 1 equiv of PPh_3 after removal of excess O_2 (shown in green, λ_{max} = 543 nm).

solution for spectroscopic monitoring (see Experimental Section). Once the bis(CO) complex (**4**) forms, it does not react with dioxygen at low temperature even in the presence of a large excess of O_2, indicating that CO is a thermodynamically stronger ligand than O_2, both for the copper and iron ion centers, as is known to occur for synthetic and natural hemes and copper complexes.[17,77,78]

While the fully reduced iron−copper complex **4** could be obtained from $[(^2L)Fe^{III}-(O_2^{2-})-Cu^{II}]^+$ (**6**) by adding CO, only a partially reduced iron−superoxo species $[(solvent)(^2L)Fe^{III}-(O_2^{-})\cdots Cu^{I}(PPh_3)]^+$ (**5**-PPh_3) was observed upon reaction of **6** with PPh_3 (Scheme 7). The UV−vis spectral changes for the **6**/PPh_3 reaction are shown in Figure 8. Addition of 1 equiv of PPh_3 to the peroxo complex $[(^2L)Fe^{III}-(O_2^{2-})-Cu^{II}]^+$ (**6**) (Figure 8, λ_{max} = 486, 546, 578 nm) yielded a new band at λ_{max} = 543 nm which is characteristic of a heme−superoxide and similar to those in $(EtCN)(F_8)Fe^{III}-(O_2^{-})$[52] and $[(EtCN)(^2L)Fe^{III}-(O_2^{-})\cdots Cu^{I}(EtCN)]^+$ (**5**) (Figure 6). This 543 nm species was stable at low temperature, which allowed further low-temperature ^2H NMR spectroscopic characterization. The pyrrole resonances for $[(^2L\text{-}d_8)Fe^{III}-(O_2^{2-})-Cu^{II}]^+$ (**6**) occur at 106 ppm in THF at −90 °C (Figure 9). Addition of 1 equiv of PPh_3 to a cold THF solution of **6** led to immediate formation of a new diamagnetic species whose pyrrole hydrogen resonances appeared at 9 ppm, a typical value for a low-spin 6-coordinate ferric−superoxide heme. Thus, the product of the reaction of **6** and PPh_3 is formulated as $[(THF)(^2L)Fe^{III}-(O_2^{-})\cdots Cu^{I}(PPh_3)]^+$ (**5**-PPh_3) on the basis of the UV−vis and NMR spectroscopic features (Scheme 7). Although direct spectroscopic detection of the $Cu^{I}-PPh_3$ group in **5**-PPh_3 is not straightforward, the formulation is well precedented; copper(I) complexes possessing the tridentate *N*,*N*-bis[2-(2-pyridyl)ethyl)]amine moiety readily form $[LCu^{I}-(PPh_3)]^+$ structures.[79,80]

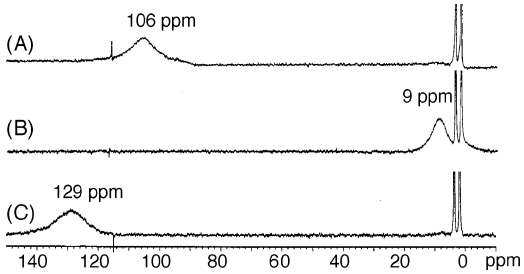

Figure 9. ^2H NMR spectra of the reaction of $[(^2L)Fe^{III}-(O_2^{2-})-Cu^{II}]^+$ (**6**) with PPh_3 in THF at −90 °C: (A) spectrum of **6** generated by bubbling $[(^2L)Fe^{II}Cu^{I}]^+$ (**3**) with O_2; (B) $[(THF)(^2L)Fe^{III}-(O_2^{-})\cdots Cu^{I}(PPh_3)]^+$ (**5**-PPh_3) generated by the reaction of **6** with 1 equiv of PPh_3 after removal of excess O_2; (C) $[(^2L)Fe^{III}-OH\cdots Cu^{I}(PPh_3)]^+$ generated by warming **5**-PPh_3 to room temperature. The sharp peaks at δ 3.58 and 1.73 ppm correspond to solvent THF.

The **6**/PPh_3 reactions were also carried out using an excess (5−10 equiv) of PPh_3. No differences in UV−vis or NMR spectral change were observed. The possible formation of $O{=}PPh_3$ from the **6**/PPh_3 was investigated using ^{31}P NMR spectroscopy because triphenylphosphine oxides are known to be generated from some reactions with iron−peroxo[81] or copper−peroxo[82] complexes with PPh_3. However, no such species was observed from the **6**/PPh_3 reaction even with a large excess (∼10-fold) PPh_3. As discussed, PPh_3 promotes the "reverse" reaction of **6** to **5** at low temperature, which then transforms to a ferric hydroxy species (λ_{max} = 575 nm, $\delta_{pyrrole}$ = 129 ppm at −90 °C) upon warming. This final "mixed-valent" thermal product was isolated in 47% yield, and it is formulated as $[(^2L)Fe^{III}OH\cdots Cu^{I}(PPh_3)]B(C_6F_5)_4$ on the basis of UV−vis and NMR spectroscopy (also having a broadened ^{31}P NMR spectrum; see also above) as well as C, H, and N elemental analysis (see Experimental Section).

Summary and Conclusion

Using a heterobinucleating ligand ^2L that contains a *N*,*N*-bis[2-(2-pyridyl)ethyl)]amine (PY2) and teteraarylporphyrine moiety, we have synthesized and characterized reduced heme and heme−copper complexes, $[(^2L)Fe^{II}]^+$ (**1**) and $[(^2L)Fe^{II}Cu^{I}]^+$ (**3**), that generate dioxygen adducts at low temperature. Complex **3** differs from previously reported heme−copper binuclear systems in having a tridentate Cu−chelate PY2 moiety, whereas the majority of known discrete heme−copper O_2 adducts are derived from systems containing a tetradentate TMPA Cu−chelate. While heme-only complex **1** binds O_2 reversibly to form a ferric−superoxo species, O_2-binding to the heme−copper complex **3** leads to the formation of a μ-η^2:η^2-bridged heme−peroxo−Cu intermediate, $[(^2L)Fe^{III}-(O_2^{2-})-Cu^{II}]^+$ (**6**). Stopped-flow kinetic studies provide insights into the oxygenation process, revealing that dioxygen initially reacts with iron to generate a transient heme−superoxo species $[(EtCN)(^2L)Fe^{III}-(O_2^{-})\cdots Cu^{I}(NCEt)]^+$ (**5**) prior to formation of **6**. Characterization of $[(^2L)Fe^{III}-$

(77) Karlin, K. D.; Zuberbühler, A. D. In *Bioinorganic Catalysis: Second Edition, Revised and Expanded*; Reedijk, J., Bouwman, E., Ed.; Marcel Dekker: New York, 1999.
(78) Karlin, K. D.; Cruse, R. W.; Gultneh, Y.; Farooq, A.; Hayes, J. C.; Zubieta, J. *J. Am. Chem. Soc.* **1987**, *109*, 2668−2679.
(79) Karlin, K. D.; Gan, Q.-F.; Farooq, A.; Liu, S.; Zubieta, J. *Inorg. Chim. Acta* **1989**, *165*, 37−39.
(80) Karlin, K. D.; Tyeklár, Z.; Farooq, A.; Haka, M. S.; Ghosh, P.; Cruse, R. W.; Gultneh, Y.; Hayes, J. C.; Toscano, P. J.; Zubieta, J. *Inorg. Chem.* **1992**, *31*, 1436−1451.
(81) Dong, Y.; Ménage, S.; Brennan, B. A.; Elgren, T. E.; Jang, H. G.; Pearce, L. L.; Que, L., Jr. *J. Am. Chem. Soc.* **1993**, *115*, 1851−1859.
(82) Paul, P. P.; Tyeklár, Z.; Jacobson, R. R.; Karlin, K. D. *J. Am. Chem. Soc.* **1991**, *113*, 5322−5332.

$(O_2^{2-})-Cu^{II}]^+$ (**6**) through reaction stoichiometry measurements, along with UV−vis, NMR, EPR, and resonance Raman spectroscopies, shows that **6** is an $S = 2$ system in which high-spin iron(III) and copper(II) ions are antiferromagnetically coupled through a bridging peroxide ligand. The fully reduced bis(carbonyl) iron(II)−copper(I) complex, $[(^2L)Fe-CO\cdots Cu-CO]^+$ (**4**), or the partially reduced iron(III)−copper(I) species, $[(solvent)(^2L)Fe^{III}-(O_2^{-})\cdots Cu^{I}(PPh_3)]^+$ (**5**-PPh_3), can be generated by adding carbon monoxide or triphenylphosphine, respectively, to the solution of $[(^2L)Fe^{III}-(O_2^{2-})-Cu^{II}]^+$ (**6**). Liberation of O_2 occurs in the carbon monoxide reaction. Neither peroxo complex **6** nor superoxo complex **5**-PPh_3 effects the oxygenation of triphenylphosphine.

Comparison of the physical properties of $[(^2L)Fe^{III}-(O_2^{2-})-Cu^{II}]^+$ (**6**) with those of other TMPA-based heme−peroxo−Cu complexes is particularly interesting because they have different peroxo-binding modes, where the former has a μ-η^2:η^2-peroxo-binding structure while some of the latter are known to possess a μ-η^2:η^1-peroxo ligation. Complex **6** has distinctive UV−vis features in the Q-band region with three absorptions at ∼485, 540, and 572 (sh) nm, whereas tetradentate systems have a major absorption band in lower energy region around 560 nm. The more dramatic difference between **6** and heme−peroxo−copper complexes with tetradentate chlelates is shown by resonance Raman spectroscopy, where a significantly lowered ν(O−O) stretching vibration occurs at 747 cm^{-1} in $[(^2L)Fe^{III}-(O_2^{2-})-Cu^{II}]^+$ (**6**). In fact, this is the lowest ν(O−O) frequency known for the heme−peroxo copper complexes, and it is ∼50 cm^{-1} lower compared to those from the tetradentate heme−peroxo−copper or the side-on bound heme-only peroxo complexes. The observed relationship between the ν(O−O) frequency and the peroxo-binding mode (i.e., end-on μ-1,2- or side-on η^2:η^2-) is analogous to that in dicopper−peroxo complexes.

Our study demonstrates that the nature of Cu^I/O_2 interactions can be applicable to the study of heme/Cu^I/O_2 reactions. It remains for future studies to see if the O−O bond weakening in $[(^2L)Fe^{III}-(O_2^{2-})-Cu^{II}]^+$ (**6**) or other systems to be investigated leads to subsequent facilitated O−O reductive bond cleavage reactions of possible relevance to cytochrome *c* oxidase.

Experimental Section

General Methods. All reagents and solvents were purchased from commercial sources and were of reagent quality unless otherwise stated. Air-sensitive compounds were handled under argon atmosphere by using standard Schlenk techniques or in a Mbraun Labmaster 130 inert-atmosphere (<1 ppm O_2, <1 ppm H_2O) glovebox filled with nitrogen. Propionitrile (EtCN) and heptane were distilled over calcium hydride under argon. Acetonitrile (CH_3CN), dichloromethane (CH_2Cl_2), tetrahydrofuran (THF), and toluene were purified over an activated alumina column under nitrogen unless otherwise noted. THF for the $[(^2L)Fe^{II}Cu^{I}]^+$ (**3**) synthesis was distilled from sodium/benzophenone under Ar. For kinetic studies, dichloromethane was distilled from calcium hydride, THF was distilled from sodium/benzophenone, and EtCN was distilled first over P_2O_5 and then over calcium hydride prior to use. Deoxygenation of these solvents was achieved by bubbling with argon for 30 min and/or (followed) by three freeze/pump/thaw cycles prior to introduction into the glovebox.

Room-temperature UV−vis spectra were obtained with a Cary 50 Bio spectrophotometer, and low-temperature UV−vis experiments were carried out using a Hewlett-packard 8453 diode array spectrometer equipped with HP Chemstation software, where the spectrometer was equipped with a variable-temperature Dewar and cuvette assembly.[78,83] IR spectra were obtained at room temperature using a Mattson Galaxy 4030 series FT-IR spectrophotometer. MALDI-TOF-MS spectra were recorded on a Kratos Analytical Kompact MALDI 4 mass spectrometer equipped with a 337 nm nitrogen laser (20 kV extraction voltage). Calibration was performed with an authentic sample of the porphyrin ligand F_8H_2. Elemental analyses were performed by Desert Analytics, Tucson, AZ (for the air-sensitive samples) or Quantitative Technologies Inc. (QTI), Whitehouse, NJ.

NMR Spectroscopy. ^1H NMR spectra at room temperature were recorded either on a Varian Unity 400 or Bruker 300 NMR instrument. Variable-temperature, T_1 measurement, and other heteronuclear NMR spectroscopic studies were carried out using a Varian Unity 400 NMR instrument. All spectra were recorded in 5-mm o.d. NMR tubes. The chemical shifts were reported as δ (ppm) values calibrated to natural abundance deuterium or proton solvent peaks for ^1H and ^2H NMR spectra, whereas phosphoric acid (0 ppm) was used as the reference for the ^{31}P NMR spectra. ^2H NMR spectra were collected using a tunable broad-band probe to enhance ^2H detection.

Solution magnetic moment measurements of $[(^2L)Fe^{III}-(O_2^{2-})-Cu^{II}]^+$ (**6**) were carried out on a Varian NMR instrument at 400 MHz (for ^1H) and 61 MHz (for ^2H). Inside a drybox, an acetone-d_6 solution of **3** with known concentration was prepared and placed in a NMR tube. A coaxial reference capillary filled with pure acetone-d_6 was then inserted inside the sample tube. A ^1H NMR spectrum of this was obtained and referenced as normal, and a ^2H NMR spectrum of the same sample was taken for an unambiguous peak assignment of the two solvent peaks, i.e., one corresponding to the paramagnetically shifted deuterated solvent peak and the second corresponding to the pure deuterated solvent from the reference capillary. The magnetic moment was calculated from the equation $\mu_B = 2.84\sqrt{x_M T/n}$, where T is the temperature (K) of the measurement, n is the nuclearity of the complex ($n = 1$ for **6**), and $\chi_M = -3/4\pi(\Delta\nu/\nu)1000/c + \chi_M^{sol} - \chi_D$ (where χ_M^{sol} is the solvent susceptibility, χ_D is the total diamagnetic correction (calculated from Pascal's constants),[84] $\Delta\nu$ is the paramagnetic shift of the solvent in Hz, ν is the frequency of the NMR instrument in Hz, and c is the concentration of the metal complex).

Electron Paramagnetic Resonance (EPR) Spectroscopy. In a glovebox, a 1 mM THF/toluene (2:1 v/v ratio; toluene to faciliate "glass" formation) solution of $[(^2L)Fe^{II}Cu^{I}]^+$ (**3**) was prepared and transferred to an EPR tube, which was capped with a rubber septum and transferred to a −95 °C cold bath (N_2/hexane). Dry dioxygen (passed through a column filled with Drierite) was added through the solution via syringe to generate $[(^2L)Fe^{III}-(O_2^{2-})-Cu^{II}]^+$ (**6**). The resulting solution was allowed to sit at −95 °C for 10 min for complete formation of **6**, after which the solution was frozen in liquid N_2 to obtain a glass. The X-band EPR spectrum of **6** was recorded on a Brucker EMX spectrometer, with temperature maintained at 15 K using an Oxford Instruments EPR 900 cryostat.

(83) Karlin, K. D.; Haka, M. S.; Cruse, R. W.; Meyer, G. J.; Farooq, A.; Gultneh, Y.; Hayes, J. C.; Zubieta, J. *J. Am. Chem. Soc.* **1988**, *110*, 1196−1207.

(84) *CRC Hand Book of Chemistry and Physics*, 80th ed.; CRC Press: London, 1999.

Resonance Raman Spectroscopy. In the glovebox, 1−5 mM THF solutions of $[(^2L)Fe^{II}Cu^{I}]^+$ (**3**) were prepared and transferred to NMR tubes (∼0.5 mL of solution/tube) and capped with tight-fitting septa. The sample tube were placed in a −95 °C cold bath (N_2/Hexane) for 10 min and oxygenated by using $^{16}O_2$, $^{18}O_2$, and $^{16/18}O_2$. ($^{18}O_2$ and $^{16/18}O_2$ gases were purchased from ICON, Summit, NJ. $^{16}O_2$ was purchased from BOC gases, Murray Hill, NJ.) The labeled gases were cooled in dry ice bath for 5 min and injected into the solution by using a Hamiltion gastight syringe. The oxygenated samples were set in a cold bath for ∼10 min, after which the sample tubes were frozen in liquid N_2 and sealed under their respective labeled O_2 atmosphere. RR spectra were collected on a McPherson 2061/207 spectrograph equipped with a liquid-nitrogen-cooled LN-1100PB CCD detector. The 413-nm laser excitation was obtained from a Coherent Innova 302 krypton laser, and the intensity at the sample was kept below 10 mW to prevent adverse effect from the laser illumination. A matching Kaiser Optical supernotch filter was used to minimize interference from the Rayleigh scattering. Frequencies were calibrated relative to several frequency standards and are accurate to ±1 cm^{-1}. To keep the sample at 90 K during data acquisition, the samples were kept in a copper coldfinger immersed in liquid nitrogen. The samples were also spun within the holder to minimize photodegradation.

Stopped-Flow Kinetics. Rapid kinetics were followed using an SF-21 variable-temperature stopped-flow unit (Hi-Tech Scientific, 2 mm path length cell) combined with a TIDAS/NMC301-MMS/16 VIS/500-1 diode array spectrometer (J & M; 256 diodes, 300−1100 nm, 0.8 ms minimum sampling time). Data acquisition (up to 256 complete spectra; up to four different time bases) was performed using the Kinspec program (J & M). For numerical analysis, all data were pretreated by factor analysis using the Specfit program.[85] To obtain variable O_2 concentrations in solution, a gas mixing unit was employed which consisted of two MKS PR-4000 control towers equipped with MKS general purpose Mass-Flo controllers of type 1179A calibrated for either 200 sccm N_2 (used for O_2 regulation) or 500 sccm N_2 (used for argon regulation). The regulated amounts of argon and O_2 were mixed which yielded a specific ratio of O_2 to argon. The mixed gases were passed through a drying column and then bubbled through the solution to yield a specific concentration of O_2 in the solvent. For the kinetic studies, CH_2Cl_2 (UVASOL, Merck) and EtCN (pa, Merck, predistilled from phosphorus pentaoxide) were distilled from calcium hydride and under argon prior to use. Thermal expansion of the solvent was taken into account.

For the reaction of $[(^2L)Fe^{II}Cu^{I}]^+$ (**3**) with O_2 in CH_2Cl_2/6% EtCN, 6 series of experiments were performed with the following room-temperature reactant postmixing concentrations ([**3**]/[O_2]/series name): 1.64×10^{-4} M/1.90×10^{-3} M/ESTA; 2.37×10^{-4} M/1.90×10^{-3} M/ESTB; 2.26×10^{-4} M/1.90×10^{-3} M/ ESTC; 1.11×10^{-4} M/1.90×10^{-3}M/ESTD; 1.10×10^{-4} M/6.00×10^{-4} M/ESTE; 2.16×10^{-4} M/6.00×10^{-4} M/ESTF. Figure 6 was made from ESTF4 which was data collected at 168 K. Data for a total of 329 individual runs between 168 and 193 K with data collection times between 0.04 and 1.48 s were obtained. Of these, 159 data sets (over a temperature range 168−179 K, where the formation of the $[(^2L)Fe^{III}-(O_2^{-})\cdots Cu^{I}]^+$ (**5**) superoxo species could be observed) were used for analysis of k_1 and 278 data sets (over the temperature range 168−191 K, where the formation of the $[(^2L)Fe^{III}-(O_2^{2-})-Cu^{II}]^+$ (**6**) peroxo species could be observed) were used for the analysis of k_2. The concentration profile based on the kinetic model $[(^2L)Fe^{II}Cu^{I}]^+$ (**3**) + O_2 → $[(EtCN)(^2L)Fe^{III}-(O_2^{-})\cdots Cu^{I}(NCEt)]^+$ (**5**) and $[(EtCN)(^2L)Fe^{III}-(O_2^{-})\cdots Cu^{I}(NCEt)]^+$ (**5**) → $[(^2L)Fe^{III}-(O_2^{2-})-Cu^{II}]^+$ (**6**), followed by (in some cases) a slow first-order relaxation, was calculated by numerical integration using the SPECFIT/32 program. Thermal expansion of CH_2Cl_2 was taken into account using r (g/mL) = $[1.48177 + 2.61843 \times 10^{-3}X - 1.7766 \times 10^{-5}X^2 + 2.38421 \times 10^{-8}X^3$, where $X = T$ (K)] for the solvent density as a function of temperature. It should be noted that the presence of 6% propionitrile was not considered to change the temperature dependence of the solvent density from that of pure CH_2Cl_2. A linear combination of the density correction factors for 6% propionitrile and 94% CH_2Cl_2 yielded results similar to those obtained using 100% CH_2Cl_2. Figure S10 shows the Eyring plot for the measurement of k_1 (the superoxo formation), and Figure S11 shows the Eyring plot for the measurement of k_2 (the peroxo formation).

For the reaction of $(F_8)Fe^{II}/[Cu^{I}(L^{Me2N})]^+$ with O_2 in CH_2Cl_2/6% EtCN (Scheme S1 in Supporting Information), three series of different $(F_8)Fe^{II}$, $[Cu^{I}(L^{Me2N})]^+$, and dioxygen concentrations were used to carry out a total of 289 measurements between −105 and +20 °C. Of these 192 were used for the final analysis. The concentrations of Fe^{II}, Cu^{I}, and dioxygen solutions used were the following: 0.15 mM Fe^{II}, 0.20 mM Cu^{I}, 1.90 mM O_2; 0.27 mM Fe^{II}, 0.39 mM Cu^{I}, 1.90 mM O_2; 0.15 mM Fe^{II}, 0.26 mM Cu^{I}, 0.63 mM O_2. Reaction time measured ranged from 1.7 to 46 s. Figure S12 shows the Eyring plot for the measurement of k_1 (the superoxo formation), and Figure S13 shows the Eyring plot for the measurement of k_2 (the peroxo formation).

Spectrophotometric Titration of $[(^2L)Fe^{III}-(O_2^{2-})-Cu^{II}]^+$ (6). In the glovebox, a known concentration (0.2−0.4 mM range in toluene/10% MeCN) of a stock solution of $[(^2L)Fe^{II}Cu^{I}]^+$ (**3**) was prepared and 2 mL of the solution was transferred to a 2 mm path length Schlenk cuvette. This was capped with a 14/24 adapter (purchased from Chemglass CG1036-14) whose opposite end was designed to fit a rubber septum. Two appropriate size rubber septa and a Teflon septum were used to seal the Schlenk cuvette from the atmosphere. The cuvette assembly was then transferred to the low-temperature UV−vis spectrometer and cooled to −75 °C. Separately, a 250 mL two sidearm Schlenk flask, whose neck was closed with a rubber septum and one sidearm was connected to an oil bubbler, was filled with 1.01% O_2 in Ar gas mixture (custom mixture purchased from Potomac Airgas, Baltimore, MD) under 1 atm pressure. A Hamilton gastight syringe equipped with a 3-way purge valve (for Ar purging of the syringe and the needle) was used to transfer known amounts of the 1.01% O_2 gas to the cold solution of **3**. To the cuvette containing a solution of **3**, was added 0.5 equiv, 1 equiv, and 2 equiv of dioxygen in three separate experiments. Each aliquot of dioxygen was bubbled directly into the solution via syringe, and the resulting solution was allowed to react until no spectral change was observed in the UV−vis spectrum (typically, it takes ∼60−70 h), after which excess dioxygen was added to the solution to reach full formation of **6** for comparison. Note that these very long reaction times are required to complete the irreversible (at these temperatures) Fe−Cu complex oxygenation reaction, when a near stoichiometric amount of O_2 gas is being added to the cuvette assembly. Whereas about half the amount of reduced starting material **3** was present with addition of 0.5 equiv of O_2, ∼90% of full formation of **6** was obtained with 1 equiv of O_2 and complete oxygenation was obtained with 2 equiv of O_2. (Consecutive addition of smaller aliquots, e.g., 0.2 equiv, of dioxygen to the same solution did not give reliable results presumably due to the relatively poor O_2-binding ability of **3** under

(85) SPECFIT/32 is a trademark of Spectrum Software Associates, copyright 2000−2002 Spectrum Software Associates (R. Binstead and A. D. Zuberbühler). Original publication: Gampp, H.; Maeder, M.; Meyer, C. J.; Zuberbühler, A. D. *Talanta* **1985**, *32*, 95−101.

the limited O_2 concentration.) Coupling this result with that of the O_2 evolution experiment of **6** with CO (see below), the reaction stoichiometry of **3**:O_2 was thus concluded to be 1:1. The spectral changes for the reaction of **6** with 1 equiv of O_2 described here are shown in the Supporting Information, Figure S6.

Detection of O_2 Evolution by Pyrogallol Solution. Evolution of dioxygen from the reaction of the $[(^2L)Fe^{III}-(O_2^{2-})-Cu^{II}]^+$ (**6**) with CO was detected using an alkaline pyrogallol solution. 1,2,3-Trihydroxybenzene (≡pyrogallol, 2 g) was placed in a 50 mL Schlenk flask that was modified to have a 1 cm path length cuvette as a sidearm, to which was added 13 mL of deoxygenated 50% KOH aqueous solution under Ar. The Schlenk flask was capped with a 14/20 joint that was sealed with triple rubber septa (see above), and the UV−vis spectrum of the solution was recorded. Using a Hamilton gastight syringe equipped with a 3-way purge valve (for Ar purging of the syringe and the needle), 6 mL of 1.01% O_2 in Ar gas mixture was added to the alkaline pyrogallol solution. The headspace of the flask and the pyrogallol solution turned brown upon addition of O_2. The flask was shaken for effective mixing for 10 min, after which the UV−vis spectrum of the solution was recorded. An additional 6 mL of 1.01% dioxygen was added followed by the same procedure, e.g., mixing and recording the UV−vis spectrum. This was repeated four more times, thereby addition of a total of 36 mL of 1.01% O_2 gas in the solution at the end. A calibration curve was generated by plotting the absorbance at 409 nm versus amount of the 1.01% O_2 added. The UV−vis spectra and the calibration curve are shown in the Supporting Information, Figure S8.

In the glovebox, to a 10 mL Schlenk flask was added a known amount (typically 11−15 mg) of $[(^2L)Fe^{II}Cu^{I}]^+$ (**3**) in 3 mL of THF. The solution was transferred to a cold bath (hexane/N_2), and the peroxo complex $[(^2L)Fe^{III}-(O_2^{2-})-Cu^{II}]^+$ (**6**) was generated by direct bubbling of dioxygen through the solution via syringe. After 10 min at −95 °C, the rubber septum of the flask was replaced with a 14/20 glass joint sealed with triple rubber septa (see above), and the excess O_2 was removed by three freeze−pump−thaw cycles. Separately, a 250 mL Schlenk flask was filled with pure CO (CO was purchased from BOC gases, Murray Hill, NJ, and used after passing through an oxygen trap OT3 which was purchased from Agilent). Using a Hamilton gastight syringe equipped with a 3-way purge valve, 20 mL of CO gas (2 × 10 mL) were added to the solution of **6** at −95 °C. The resulting solution was allowed to warm to room temperature. In the meantime, 13 mL of alkaline pyrogallol solution was freshly prepared in a modified 50 mL Schlenk flask possessing a 1 cm path length cuvette. A short vacuum tubing was attached to the sidearm of each Schlenk flask (one containing the pyrogallol solution, the other containing the reaction mixture of **6** plus CO). Then, the two flasks were connected to a three-way glass stopcock whose third arm was connected to a standard Schlenk line (the other two arms are connected via vacuum tubing to the Schlenk flasks). After ensuring that the connecting vacuum tubing was under inert atmosphere, the headspace of the 50 mL Schlenk flask which contains the pyrogallol solution was placed under static vacuum, after which the three-way glass stopcock and the sidearm stopcocks of the Schlenk flasks were opened so that the two flasks were connected but they were isolated from the atmosphere. The pyrogallol solution immediately turned brown. The two flasks were allowed to sit for 2 h, and the UV−vis spectrum of the resulting solution was recorded. The amount of O_2 evolved was calculated from the calibration curve described above (Figure S8, Supporting Information). Three reaction runs produced 63%, 65%, and 80% yields.

Reactions of $[(^2L)Fe^{III}-(O_2^{2-})-Cu^{II}]^+$ (6) with Triphenylphosphine. (a) UV−Vis Analysis. The reaction of **6** with 1, 5, and 10 equiv of triphenylphosphine was monitored by UV−vis spectroscopy in the presence and the absence of excess O_2. Inside the glovebox, typically a 0.3−0.5 mM solution of $[(^2L)Fe^{II}Cu^{I}]^+$ (**3**) was prepared and 4 mL of the stock solution was transferred to a Schlenk cuvette that was capped with a rubber septum. The sample was brought to the low temperature in a UV−vis spectrometer and cooled at −80 °C. The peroxo complex **6** was generated by bubbling dioxygen through the solution of **3**. If needed, excess O_2 was removed by 10 cycles of vacuum/Ar purge. Separately, a triphenylphosphine stock solution (30−50 mM) was prepared inside the glovebox, and a proper amount of the solution was taken using a microsyringe, which then was added to the cold solution of **6**. The spectral changes are shown in Figure 8.

(b) ^{2}H NMR Analysis. The reaction of **6** with 1 equiv triphenylphosphine was followed by low-temperature ^{2}H NMR spectroscopy. Inside the glovebox, a THF solution of $[(^2L\text{-}d_8)Fe^{II}Cu^{I}]^+$ (**3**) (11 mg of **3** in 0.5 mL of THF) was prepared inside a 5 mm NMR tube, and the tube was transferred to a −95 °C cold bath (hexane/N_2). **6** was generated by direct bubbling O_2 through the solution via syringe. Complete formation of **6** was confirmed (by ^{2}H NMR spectroscopy as well) prior to adding triphenylphosphine. A 1 equiv amount of PPh_3 solution was directly added to the solution **6** via syringe at −95 °C, after which the NMR spectrum was recorded at −90 °C. The ^{2}H NMR spectra described here are shown in Figure 9.

(c) ^{31}P NMR Analysis. The reaction of **6** with 2 equiv of triphenylphosphine was followed by ^{31}P NMR spectroscopy at room temperature. In a 10 mL Schlenk flask equipped with a magnetic stir bar, **6** was generated by direct O_2 bubbling through solution of **3** (15 mg of **3** in 3 mL of acetone-d_6) at −93 °C. The excess dioxygen was removed by 10 cycles of vacuum/Ar purging. A 2 equiv amount of PPh_3 solution (in acetone-d_6) were added to **6** via syringe under Ar. The resulting reaction mixture was stirred for 1 h at −93 °C, which then was allowed to warm to room temperature. After concentration of the solution under vacuum to approximately 0.5 mL, the solution was transferred to a NMR tube and the ^{31}P NMR spectrum was recorded. No signal for triphenylphosphine oxide was observed. A significantly broadened ^{31}P resonance from triphenylphosphine appeared at −2.0 ppm (Figure S9, Supporting Information), which was downfield shifted from that of an authentic PPh_3 (−4.1 ppm). Dynamic behavior between free PPh_3 and copper-bound PPh_3 may be present in the sample, which could cause the line broadening and the change of the chemical shift. To test this possibility, the ^{31}P NMR spectrum of $[Cu^{I}(L^{H})(PPh_3)]^+$ was recorded. An extremely broad ^{31}P resonance was found at 3 ppm in acetone-d_6.

Synthesis. $(F_8)Fe^{II}\cdot H_2O$,[23,60] $[(L^{H})Cu^{I}]B(C_6F_5)_4$,[21,2] LH_2, $(^2L)Fe^{II}\cdot$THF (**1**·THF),[19] and $[(^2L)Fe^{II}Cu^{I}]B(C_6F_5)_4\cdot THF\cdot H_2O$ (**3**·THF·H_2O)[19] were synthesized according to published procedures.

$F_6(NO_2)TPPH_2$-d_8, 5,10,15-Tris(2,6-difluorophenyl)-20-(2-nitrophenyl)porphyrine-d_8. To a 1 L round-bottom flask equipped with a magnetic stir bar was added 400 mL of propionic anhydride, 56 mL of deuterium oxide, and 12 g (0.18 mol) of pyrrole. The mixture was brought to reflux for 1 h under Ar, after which 2-nitrobenzaldehyde (7.6 g, 0.05 mol) and 2,6-difluorobenzaldehyde (12.5 g, 0.09 mol) and 100 mL of nitrobenzene were added through the top of the condenser. The reaction mixture was allowed to reflux with stirring for an additional 1.5 h. The solution was cooled to room temperature, opened to the air, and stored in a freezer (−15 °C) for 2 days. The cold reaction mixture was filtered over Celite, and the precipitate (porphyrins) was washed with 3 L of distilled

water, after which the precipitate and the Celite were rinsed with CH_2Cl_2 (2 L). The filtrate was saved and dried over sodium sulfate for 1 h. After removal of the solvent on the rotary evaporator, the crude product was purified by column chromatography (silica, 1:1 CH_2Cl_2:hexane, $R_f = 0.2$), yielding 1 g (0.0014 mol, 5%) of the desired product. By ^{1}H NMR analysis, ∼85% of the β-pyrrolic hydrogens were determined to be deuterated. ^{1}H NMR (300 MHz, $CDCl_3$): δ (ppm) 8.67−8.86 (m, 1.2 H), 8.45 (d, 1H), 8.21 (d, 1H), 7.86−7.96 (m, 2H), 7.72−7.82 (m, 3H), 7.32−7.40 (m, 6H), −2.70 (s, 2H).

[(^{2}L)Fe^{III}−OH···Cu^I(PPh$_3$)]B(C$_6$F$_5$)$_4$·THF·3H$_2$O. Inside the glovebox, 45 mg (0.024 mmol) of [(^{2}L)Fe^{II}Cu^I]B(C$_6$F$_5$)$_4$·THF·H$_2$O (**3**·THF·H$_2$O) was placed in a 50 mL Schlenk flask, to which was added 5 mL of deoxygenated THF. The flask was capped with a rubber septum and brought to a −95 °C bath (hexane/N_2), after which dry dioxygen was bubbled through the solution of **3**. The resulting solution was allowed to sit at −95 °C for 15 min to ensure complete formation of [(^{2}L)Fe^{III}−(O_2^{2-})−Cu^{II}]$^+$ (**6**). Excess dioxygen was removed by application of 10 cycles of vacuum/Ar purge. Then, 1 equiv of triphenylphosphine (6.3 mg in 200 μL) was added to the solution via syringe. The resulting mixture was allowed to sit at −95 °C for 15 min, followed by warming to room temperature. The solution was concentrated in vacuo to ∼3 mL, after which 35 mL of deoxygenated pentane was added to precipitate the product. After decanting of the supernatant, the solid was dried under vacuum, yielding 25 mg (0.011 mmol, 47% yield) of [(^{2}L)Fe^{III}−OH···Cu^I(PPh$_3$)]B(C$_6$F$_5$)$_4$·THF·3H$_2$O as a purple solid. Anal. Calcd for C$_{107}$H$_{72}$O$_6$BN$_8$F$_{26}$FeCuP: C, 57.87; H, 3.27; N, 5.05. Found: C, 57.86; H, 3.08; N, 4.59. UV−vis [THF; λ_{max}, nm; room temperature]: 335, 413, 565.

Acknowledgment. This work was supported by the National Institutes of Health (K.D.K. (Grant GM 60353), P.M.-L (Grant GM18865), postdoctoral fellowships to M.E.H. (Grant GM20805)), and the Swiss National Science Foundation (A.D.Z.). We are also thankful to Dr. Marie-Aude Kopf for initial observations made in a similar system.

Supporting Information Available: An X-ray crystallographic data file (CIF), UV−vis and ^{2}H NMR spectra of **1**/O_2, ^{2}H NMR spectra of **3**, O_2 titration (UV−vis monitored) of **3**, UV−vis and IR spectra of **6**/CO, UV−vis spectral change of an alkaline pyrogallol solution upon stepwise additions of O_2, ^{31}P NMR spectra of [(^{2}L)Fe^{III}−OH···Cu^I(PPh$_3$)]$^+$, and kinetics Eyring plots. The material is available free of charge via the Internet at http://pubs.acs.org.

IC050446M